Transit Timing and Duration Variations for the Discovery and Characterization of Exoplanets in the TESS Era





Transit Timing and Duration Variations for the Discovery and Characterization of Exoplanets in the TESS Era

Eric Agol and Daniel C. Fabrycky

Contents

Introduction	2
Preliminaries	6
Theory and Paradigmatic Examples	8
Chopping	11
Transit Duration Variations	11
Observational Considerations: Timing Precision	13
Science Results	15
Recent Theoretical Developments	18
Transit Timing in the TESS Era	20
Transit Timing Versus Radial Velocity	22
Transit Timing with HST and JWST	25
A Prescription for Transit Timing/Duration Analyses	26
Unsolved Problems and Future Developments	28
Cross-References	30
References	30

Abstract

Transiting exoplanets in multi-planet systems have non-Keplerian orbits which can cause the times and durations of transits to vary. The theory and observations of transit timing variations (TTV) and transit duration variations (TDV) are reviewed. The *Kepler* spacecraft has detected several hundred perturbed

E. Agol (\boxtimes)

Department of Astronomy, University of Washington, Seattle, WA, USA e-mail: agol@uw.edu; agol@astro.washington.edu

D. C. Fabrycky

Department of Astronomy and Astrophysics, University of Chicago, Chicago, IL, USA e-mail: fabrycky@uchicago.edu

planets, many of which are still undergoing further study, and now, TESS is adding to this sample. In a few cases, these data have been used to discover additional planets, similar to the historical discovery of Neptune in our own solar system. However, the more impactful aspect of TTV and TDV studies has been characterization of planetary systems in which multiple planets transit. After addressing the equations of motion and parameter scalings, the main dynamical mechanisms for TTV and TDV are described, with citations to the observational literature for real examples. Constraints on model parameters from timing are elucidated, particularly the origin of the mass/eccentricity degeneracy and how it is overcome by the high-frequency component of the signal. On the observational side, derivation of timing precision and introduction to the timing diagram are given. Science results are reviewed, with an emphasis on mass measurements in multi-transiting planetary systems, from which bulk compositions may be inferred. The progress being made in studying transit timing with TRAPPIST-1 and TESS multi-planet systems is reviewed, as well as what the future may hold.

Introduction

Transit timing variations (TTV) and transit duration variations (TDV) are two of the newer tools in the exoplanetary observer's toolbox for discovering and characterizing planetary systems. Like most such tools, they rely on indirect inferences, rather than detecting light from the planet directly. However, the amount of dynamical information they encode is extremely rich.

To decode this information, let us start with the dynamical concepts. Consider the vector stretching from the star of mass m_0 to the planet of mass m to be $\mathbf{r} = (x, y, z)$, with a distance r and direction $\hat{\mathbf{r}}$. The Keplerian potential per reduced mass, $\phi = -GM/r$ (where $M \equiv m_0 + m$ and the planet is replaced with a body of reduced mass $\mu \equiv m_0 m/M$), gives rise to closed orbits. This means that, in the absence of perturbations, the trajectory is strictly periodic, $\mathbf{r}(t+P) = \mathbf{r}(t)$. Moreover, Kepler showed that Tycho Brahe's excellent data for planetary positions were consistent with Copernicus' idea of a heliocentric system only if the planets (including the Earth) followed elliptical paths of semimajor axis a, and one focus on the sun. Newton was successful at finding the principle underlying such orbits, a force law $\mathbf{F} = \mu \ddot{\mathbf{r}} = -G\mu m_0 r^{-2} \hat{\mathbf{r}}$, which results in a period $P = 2\pi a^{3/2} (GM)^{-1/2}$ (i.e., with the a-scaling Kepler found the planets actually obeyed).

This research program was thrown into some doubt by the "Great Inequality," the fact that the orbits of Jupiter and Saturn did not fit the fixed Keplerian ellipse model. This obstacle was overcome by the perturbation theory of Laplace, who used the masses derived via their satellite orbits to explain the deviations of their heliocentric orbits (Wilson 1985). The insight can be calculated by writing an additional force to that of gravity of the sun:

$$\mathbf{F_1} = \mu_1 \ddot{\mathbf{r}}_1 = -G\mu_1 M r_1^{-2} \hat{\mathbf{r}}_1 + \mathbf{F}_{12},\tag{1}$$

where now the forces and distances specifically pertain to planet 1 and a force of planet 2 on planet 1 is added. This latter force consists of two terms:

$$\mathbf{F_{12}} = G\mu_1 m_2 |r_2 - r_1|^{-3} (\mathbf{r_2} - \mathbf{r_1}) - G\mu_1 m_2 r_2^{-2} \hat{\mathbf{r_2}}.$$
 (2)

The first term on the right-hand side is the direct gravitational acceleration of planet 1 due to planet 2. The second is an indirect frame-acceleration effect, due to the acceleration the star feels due to the second planet. Since the sun is fixed at the zero of the frame, this acceleration is modelled by acceleration of planet 1 in the opposite direction. This F_{12} force can be used to account for the Great Inequality with the interactions of Jupiter and Saturn.

Likewise, Leverrier and Adams used planet-planet perturbations in the first discovery of a planet by gravitational means (Adams 1847; Le Verrier 1877). In this case, they did not know the zeroth order solution (i.e., the Keplerian ellipse) for the perturber, Neptune. In its place, they assumed the Titius-Bode rule held and sought only the phase of the orbit. This technique worked because they only wanted to see how the acceleration, and then deceleration, of Uranus as it passed Neptune, would betray Neptune's position on the sky to optical observers. The task of discovering planets by TTV is more demanding as one does not have any hints as to what the planet's orbit might be, i.e., one cannot assume it is on a circular orbit or obeys some spacing law. The observation of a single orbit is insufficient for a detection: times of at least three transits are needed to measure a period change. However, due to measurement error, in only a small fraction of cases is the high-frequency "chopping" signal (see Chopping section below) statistically significant after just three transits. Moreover, the sampling of the orbit only at transit phase causes aliasing of the dynamical signals (Kipping 2020).

The times of transit are primarily constrained by the decline of stellar flux during transit ingress, and the rise over egress, which occur on a timescale

$$\tau \approx \pi^{-1} P(R_p/a) \approx 2.2 \min\left(\frac{R_p}{R_{\oplus}}\right) \left(\frac{m_0}{M_{\text{sun}}}\right)^{-1/3} \left(\frac{P}{10d}\right)^{1/3},\tag{3}$$

assuming a circular orbit, edge on to the line of sight (impact parameter of b=0), around a star of mass m_0 ; usually, timing precision can be measured better than this timescale. This timing precision gives a sensitive measure of the variation of the angular position of a planet relative to a Keplerian orbit. In contrast, the other dynamical techniques rely on a signal spread through the orbital timescale P, and thus, the precision of the orbital phase is poorly constrained unless the measurements are of high precision or long duration (although these conditions have been achieved by pulsar timing in PSR 1257 +12 which detected a Great Inequality, Wolszczan 1994, and by radial velocity in GJ 876 which detected resonant orbital precession, Laughlin and Chambers 2001).

Orbital positions or transit times are expressed in a table called an ephemeris. Perturbations cause motions or timing deviations from a Keplerian reference model, especially changes to its instantaneous semimajor axis a, eccentricity e, time of

periastron passage t_p , and longitude of periastron ω . The latter angle is between the position of closest approach and a plane perpendicular to the line of sight that contains either the primary body or the center of mass. In the case of transit timing variations, the Keplerian alternative is simply an ephemeris with a constant transit period, P:

$$C = T_0 + P \times E, \tag{4}$$

where E is the epoch – an integer transit number – and T_0 is the time of the transit numbered E=0; C stands for "calculated" based on a constant-period model. Meanwhile, the observed times of transit are denoted O. This notation leads to an O-C (pronounced "O minus C"; Sterken 2005) diagram, in which only the perturbation part is plotted. An instructive version, modelled after the timing of TOI-2015b (Jones et al. 2024) but with a greatly exaggerated perturbation, is shown in Fig. 1. The transit times come earlier than the linear model for transit numbers 0–36, 97–151, and 212–263 and later than the linear model for the remaining transits. These deviations from a constant transit period are what astronomers call TTVs.

The other dynamical effect addressed by this review is TDVs. Like TTVs, the cause can be changes in a, e, or ω . The most dramatic effect, however, is due to orbital plane reorientation. The angle the orbital plane's normal vector makes to the observer's line of sight – the inclination, i – determines the length of the transit chord. Changes in the inclination will change the length of that chord, which in turn changes the amount of time the planet remains in transit: duration variations.

The literature on exoplanets has a history of rediscovering effects that had been well studied in the field of binary and multiple stars. In the current focus, it has long been known to eclipsing binary observers that long-term depth changes can result from the torque of a third star orbiting the pair (Mayer 1971). This effect owes to the secular and tidal dynamics which dominate triple star systems (Borkovits et al. 2003, 2011), dictated by their hierarchical configuration which allows them to remain stable. TDV due to perturbing planets is simply its exoplanetary analogue (Miralda-Escudé 2002).

The first recognition of the importance of transit timing and duration variations was at the DPS and AAS meetings almost three decades ago by Dobrovolskis and Borucki (1996a,b), followed a few years later by Miralda-Escudé (2002) and Schneider (2003, 2004). More detailed studies that included the important effect of mean-motion resonance, in which the ratio of two planets' orbital periods is close to the ratio of small integers, were independently investigated by Holman and Murray (2005) and Agol et al. (2005). The former paper showed that solar system-like perturbations might be used to find earthlike planets, should transit times be measured with sufficient accuracy. The latter paper coined the term "transit timing variations," with acronym TTV, and defined TTVs as the observable accumulation of transit period changes (i.e., O - C).

Initial studies of TTVs of hot Jupiters were able to place limits on the presence of Earth-mass planets near mean-motion resonance (Steffen and Agol 2005). Some further studies claimed detection of perturbing planets causing TTVs or TDVs, but

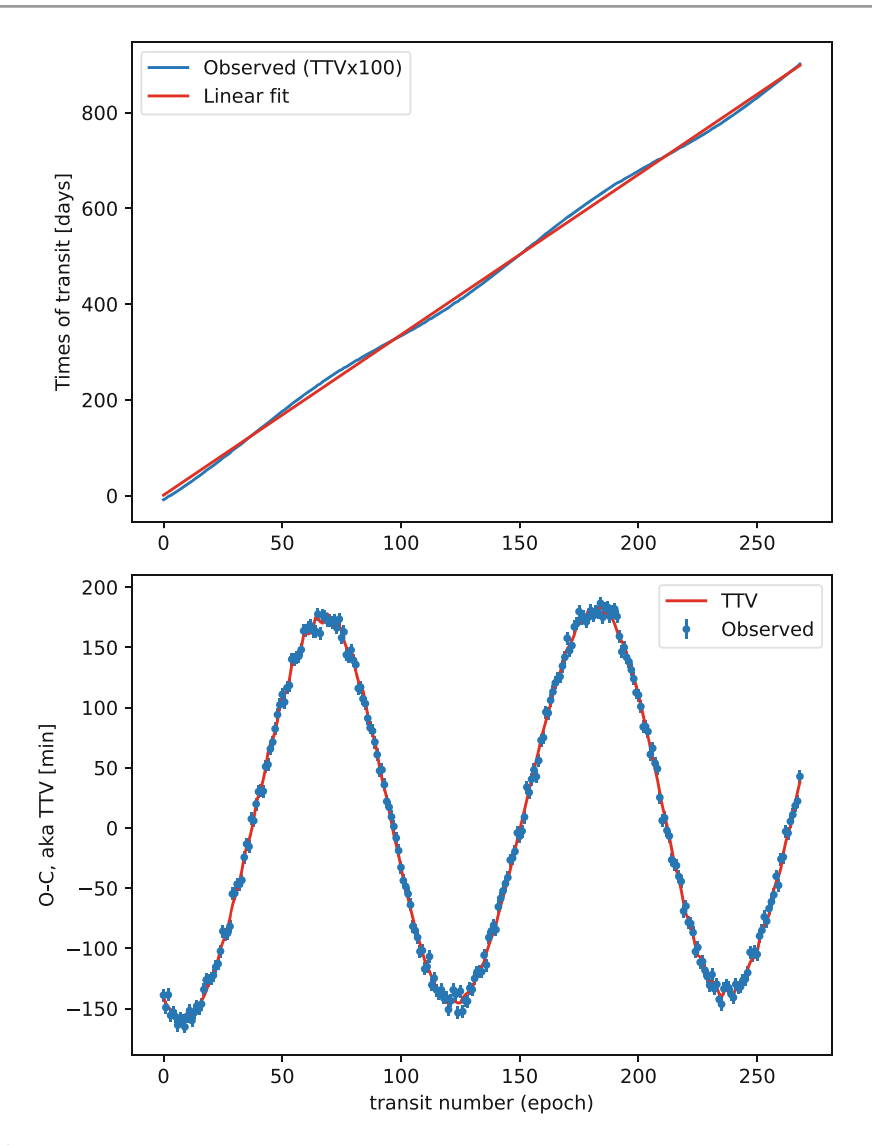


Fig. 1 An example of simulated timing data with added 5-minute normal white noise. *Top panel*: the "measured" midtimes of exoplanet transits (blue; the TTVs have been exaggerated by a factor of 100 in this panel to make them visible by eye), to which a line is fit by least squares (red). *Bottom panel*: the residuals of the linear fit (blue error bars), which is the conventional observed minus calculated (O-C) diagram; the original noise-free TTVs are also plotted as a red curve

each of these were quickly disputed or refuted by additional measurements. The first convincing detection awaited the launch of the *Kepler* spacecraft and the discovery of Kepler-9 which showed large-amplitude TTVs of two Saturn-sized planets with strong significance (Holman et al. 2010); this discovery was remarkably similar to

predictions based upon the GJ 876 system (Agol et al. 2005). The Kepler-9 paper kicked off a series of discoveries of TTVs with the *Kepler* spacecraft, with now more than 375 planets displaying TTVs, according to the Confirmed Planets table in the NASA Exoplanet Archive on 12/5/2024, and some showing TDVs (Holczer et al. 2016). Although most TTV detections have been space based, the first ground-based detections were made for TRAPPIST-1 (Gillon et al. 2017) and WASP-148 b (Hébrard et al. 2020).

Preliminaries

Since the gravitational interactions between planets occur on the orbital timescale, the amplitude of TTVs is proportional to the orbital period of each planet, times a function of other dimensionless quantities. Thanks to Newton's second law and Newton's law of gravity, the acceleration of a body does not depend on its own mass. Thus, the TTVs of each planet scale with the masses of the *other* bodies in the system. In a two-planet system, then, to lowest order in mass ratio, the O-C formulae are

$$\delta t_1 = P_1 \frac{m_2}{m_0} f_{12}(\alpha_{12}, \boldsymbol{\theta}_{12}),$$

$$\delta t_2 = P_2 \frac{m_1}{m_0} f_{21}(\alpha_{12}, \boldsymbol{\theta}_{21}),$$
(5)

where the masses of the star and planets are m_0, m_1 , and m_2 and f_{ij} describes the perturbations of planet j on planet i, which is a function of the semimajor axis ratio, $\alpha_{ij} = \min(a_i/a_j, a_j/a_i)$, and the angular orbital elements of the planets, $\theta_{ij} = (\lambda_i, e_i, \omega_i, I_i, \Omega_i, \lambda_j, e_j, \omega_j, I_j, \Omega_j)$. The evaluation of these functions can be found in a series of papers on perturbation theory: Nesvorný and Morbidelli (2008), Nesvorný (2009), Nesvorný and Beaugé (2010), Lithwick et al. (2012), Nesvorný and Vokrouhlický (2014, 2016), Agol and Deck (2016), Deck and Agol (2016), Hadden and Lithwick (2016), and Judkovsky et al. (2022a).

With the addition of multiple perturbing planets, if the mass ratios of the planets to the star are sufficiently small and if none of the pairs of planets are in a mean-motion resonance, then the TTVs may be approximately expressed as linear combinations of the perturbations due to each companion. For *N* planets, the TTVs become

$$\delta t_i = P_i \sum_{j \neq i} \frac{m_j}{m_0} f_{ij}(\alpha_{ij}, \boldsymbol{\theta}_{ij}), \tag{6}$$

for i = 1, ..., N.

The largest TTVs are caused by orbital period changes associated with libration of the system about a mean-motion resonance. Energy trades can be used to compute the amplitude of the TTV in each planet (see Agol et al. 2005; Holman et al. 2010).

Because of Kepler's relation $a \propto P^{3/2}$, a period lengthening of $\delta P_1 \ll P_1$ is associated with a semimajor axis change of $\delta a_1 = (3/2)a_1\delta P_1/P_1$. Differentiating the orbital energy equation $E_1 = -GMm_1/(2a_1)$ shows that such a change results in an energy change of $\delta E_1 = (GMm_1a_1^{-2}/2)\delta a_1$. To conserve total energy, the other planet will have an energy change of $\delta E_2 = -(GMm_1a_1^{-2}/2)\delta a_1$, which can also be expressed as $+(GMm_2a_2^{-2}/2)\delta a_2$. Using the relation $\delta a_2 = (3/2)a_2\delta P_2/P_2$ and the Keplerian relation $a_2/a_1 = (P_2/P_1)^{2/3}$, one obtains

$$\delta P_2 = -\delta P_1 (m_1/m_2) (P_2/P_1)^{5/3}. \tag{7}$$

When considering the O-C shapes that each planet makes over a fixed time interval (e.g., from a survey that measures transits for both planets), there will be a factor of P_2/P_1 more orbital periods for the inner planet than the outer planet. Thus, the accumulated time shift of the signal, δt , builds up more for the inner planet, by one factor of the period ratio. In consideration of Eq. 7, one is left with

$$\delta t_2 = -\delta t_1 (m_1/m_2) (P_2/P_1)^{2/3}. \tag{8}$$

This scaling agrees with analytic work performed in the resonant (Nesvorný and Vokrouhlický 2016) and near-resonant (Lithwick et al. 2012; Hadden and Lithwick 2016) regimes. Hence, the TTV curves of the two planets are often anticorrelated, with the ratio of planetary masses determining the ratio of TTV amplitudes. In the case that the masses are equal, the amplitude of the outer planet's TTV is larger because its orbital size needs to change more for its Keplerian orbital energy to equal the change in the inner planet's Keplerian orbital energy.

In general, transit timing variations afford a means of measuring the density of exoplanets. The two observables associated with a light curve are the time stamp of each photometric measurement and the number of photons measured. The number of photons is a dimensionless number and thus may only constrain dimensionless quantities, such as radius ratio, impact parameter, or the ratio of the stellar size to the semimajor axis. The quantities that have units of time – the period, transit duration, and ingress duration – can constrain the density of the system since the dynamical time relates to stellar density, ρ , as $t_{dyn} \approx (G\rho)^{-1/2}$. Seager and Mallén-Ornelas (2003) showed that a single transiting planet on a well-measured circular orbit may be used to gauge the density of the star; in the case of multiple transiting planets, the circular assumption may be relaxed (Kipping 2014).

The transit depth, then, gives the radius ratio of the planet to the star, while if two planets transit and show TTVs, their TTVs give an estimate of the mass ratio of the perturbing planet to the star. Thus, two transiting, interacting planets yield an estimate of the density ratio of the planets to the star, and consequently, one obtains the density of the planets. Note that this is true even if the absolute mass and radius of the star are poorly constrained. A caveat to this technique is that there is an eccentricity dependence that is present in the stellar density estimate. However, multi-transiting planet systems typically require low eccentricities to be

stable, and in some cases, the eccentricities can be constrained sufficiently from TTV analysis, from analyzing multiple planets (Kipping 2014), or from statistical analysis of an ensemble of planets (Hadden and Lithwick 2017). So, this caveat ends up not impacting the stellar density estimate significantly (the mass-eccentricity degeneracy, however, reduces precision on planet-star mass ratios and hence inflates the planet density uncertainty). Another way to obtain an estimate of stellar density is from asteroseismology: in fact, the time dependence of asteroseismic measurements is what enables density to be constrained in that case as well (Ulrich 1986). More recently, the Gaia spacecraft has measured accurate parallaxes, which can yield stellar parameters when combined with photometric and spectroscopic data (Berger et al. 2018; Fulton and Petigura 2018), including density.

Theory and Paradigmatic Examples

This section reviews the physical models for different types of TTV interactions and points the reader to real systems that exhibit each kind of interaction.

Close to resonances, a combination of changes in semimajor axis and eccentricity leads to TTV cycles whose period depends on the separation from the resonance (Steffen 2006; Lithwick et al. 2012); the latter refer to this as the "super-period." The dominant TTV variation comes from only one resonance, the one the system is closest to, which allows its critical angles to move slowly and thus its effect to build up. If the period ratio P_2/P_1 is within a few percent of the ratio j/k, with j and k being integers, then the expected TTV period is

$$P_{\text{TTV}} = 1/|j/P_2 - k/P_1|. \tag{9}$$

The order of the resonance is |j-k|, and the strength of the resonant TTV depends on the planetary eccentricities to a power of the order minus 1 (Lithwick et al. 2012; Agol and Deck 2016; Deck and Agol 2016). Therefore, first-order resonances affect planets with no initial eccentricity, but higher-order resonances have a large effect only in the presence of some eccentricity.

Seeing two planets transit the star helps immensely to characterize a near-resonant system, because then the relative transit phase of the two planets can be compared with the phase of the TTV signals (Lithwick et al. 2012). If the eccentricities are maximally damped out, then the resonant terms of the interaction continue forcing a small eccentricity that quickly precesses, causing the TTV. In this case, the phase of the signal is predictable, and the two planets' eccentricities are anti-aligned, so the TTV signals consist of anticorrelated sinusoids. Also useful in this case is that the amplitudes lead directly to the planetary masses. If the so-called free eccentricity remains, however, the phases would usually differ from that prediction, the TTV in the two planets may not be in perfect antiphase, and only an approximate mass scale rather than a measurement is available, which is referred to as the mass-eccentricity degeneracy. The first real system that showed this pattern

convincingly was Kepler-18 (Cochran et al. 2011). The degeneracy between mass and eccentricity results from sampling at the period of the transiting planet, which causes short period variations to be aliased with $P_{\rm TTV}$ (Lithwick et al. 2012; Deck and Agol 2015).

The measurement of TTVs and TDVs has been used for confirmation, detection, and characterization of transiting exoplanets and their companions. The *Kepler* spacecraft discovered thousands of transiting exoplanet candidates; the classification as "candidate" was cautiously used to allow for other possible explanations, such as a blend of a foreground star and a background eclipsing binary causing an apparent transit-like signal. The presence of multiple transiting planets around the same star gave a means of confirming two planets that display *anticorrelated* TTVs: due to energy conservation (Eq. 8), the anticorrelation indicates dynamical interactions between the two planets, while such a configuration would not be stable for a triple star system. Many papers used this technique to confirm that *Kepler* planet candidates were bona fide exoplanets using different techniques to identify the anticorrelation in data (Ford et al. 2012a,b; Fabrycky et al. 2012; Steffen et al. 2012a; Xie 2013).

Beyond confirmation and detection, characterization of exoplanets with TTVs also began in earnest with the *Kepler* spacecraft. In addition to Kepler-9, the Kepler-18 system was characterized by a combination of TTVs and RVs, giving density estimates for the three transiting planets (Cochran et al. 2011) and assuring that the new method for mass characterization gave the same answers as the trusted, older method.

When only one planet transits in a near-resonant system, the measured TTVs may simply record a sinusoidal signal, which could result from the other planet being close to many different resonances with the transiting planet (Meschiari and Laughlin 2010). In Kepler-19, Ballard et al. (2011) were able to tell that a planetary companion was the only sensible cause of the TTV, but they were not able to break this finite set of degeneracies; nevertheless, this constituted the first detection of an exoplanet with TTVs. This companion was confirmed, and its period and mass were determined, by Malavolta et al. (2017).

This degeneracy has made it extremely difficult to characterize non-transiting planets via TTV, and hence, in many cases, an additional planet is suspected due to TTV, but detailed work has not been pursued to determine its nature. The first case of a non-transiting planet being discovered *and* completely characterized was Kepler-46 (aka KOI-872; Nesvorný et al. 2012). The authors found that the TTVs of the transiting planet were far from a sinusoidal shape; in fact, they could be Fourier decomposed into at least four significant sinusoids. Each of these sinusoids can be identified as the interaction with the non-transiting planet via a different resonance. Even with all this extra information, TTVs could only narrow down the possible perturbing planets to a degenerate set of two, and below is described how TDVs broke this degeneracy.

Planets that are truly in resonance with each other have the largest TTV signals. On a medium-baseline timescale like that of *Kepler*, they can perturb each other's

orbital periods. The resonant interaction traps the planets at a specific period ratio, causing the periods to oscillate near that ratio. The period of the full cycle of that oscillation depends on the ratio of the planet masses to the host star's mass, to the -2/3 power (Agol et al. 2005; Nesvorný and Vokrouhlický 2016). For instance, the touchstone system GJ876 has a 550 day libration cycle, about ten times the outer planet's period, due to its relatively massive planets and low-mass star. A system which was characterized by resonant interaction is KOI-142 (Nesvorný et al. 2013), in which a non-transiting planet was discovered. A system with two transiting planets in resonance with large TTVs is Kepler-30 (Fabrycky et al. 2012). A system with smaller libration amplitudes but a surprising *four* planets in resonance (forming a chain of resonances) is Kepler-223 (Mills et al. 2016). Dawson et al. (2021) showed that TOI-216 b/c are in resonance with a joint analysis of the RV and TTVs.

Several other TTV mechanisms have been detected which do not rely on resonances but are relevant for more hierarchical situations $(P_2/P_1 \gtrsim 4)$.

If the outer planet transits, and the inner orbiting body is very massive, the dominant effect can be the shifting of the primary star with respect to the barycenter. Then, as the outer planet orbits the barycenter, it arrives at the moving target either early or late. This effect was numbered (i) by Agol et al. (2005), and it is seen clearly in circumbinary planet systems. For instance, the secondary star of Kepler-16 (Doyle et al. 2011) moves the primary by many times its own radius, resulting in an \sim 8 day TTV on top of a 225 day orbit. Millholland et al. (2016) have detected a candidate hot Jupiter, KOI-1822.02, using TTVs induced on an outer transiting companion by reflex motion of the host star, in addition to a phase variation.

A final mechanism of dynamical TTV is relevant for the inner orbit when a massive body orbits at large distance. The tide that body exerts on the inner orbit causes its orbital period to differ slightly from what it would be in the absence of that outer body. If the outer body is in the plane of the inner orbit, its tide slows down the inner orbit, lengthening its period. If the outer body is far out of the plane of the inner orbit, its tide speeds up the inner orbit, shortening its period. The tide also depends on the third power of the distance to that external body. Hence, when the external body moves on an eccentric and/or inclined orbit, it induces a period variation in the inner orbit, which has the period of the outer orbit. Also important for the timing is how the outer perturber instantaneously torques the inner orbit's eccentricity. These effects were put together and analyzed by Borkovits et al. (2003) in the context of triple star systems and the in-plane physics was explained as mechanism (ii) of Agol et al. (2005). An example of these effects was provided by Kepler-419 (Dawson et al. 2014), in which an eccentric massive planet accompanies an inner planet with a period ratio of 9.7. A highly eccentric, long-period ($P \approx 225$ d) transiting Jupiter found with TESS, TOI-4562b, shows TTVS which may be explained by a perturbing companion with a period of 3990 d or nearly 11 years, TOI-4562 c (Heitzmann et al. 2023; Fermiano et al. 2024). If confirmed, this detection may set a record both for the period ratio of an outer planet found with TTVs $(P_c/P_b \approx 17)$ and for the absolute orbital period of the companion, $P_c \approx 11$ yr. Such a massive planet with long orbital period may be detectable with Gaia (Heitzmann et al. 2023), which would enable an estimate of the mutual inclination of these two giant planets.

Chopping

When two planets are nearly resonant, the degeneracy between the mass ratios of the planets to the star and the eccentricity vector may be broken by examining additional TTV components present in the data (Deck and Agol 2015). Nonresonant perturbations occur on the time from one conjuction of the planets to the next, which is when their separation is smallest and gravitational attraction is strongest. Conjunctions occur on a period of $P_{\text{syn}} = (1/P_1 - 1/P_2)^{-1}$, also referred to as the synodic period. TTVs at the synodic period, and its harmonics, have smaller amplitude due to the fact that they do not always add coherently and thus require higher signal to noise to detect. These synodic variations are referred to as "chopping" as they commonly show TTVs that alternate early and late, on top of the larger amplitude TTVs with period P_{TTV} . Despite the smaller amplitude, the chopping components can be detected in many cases and can break the mass-eccentricity degeneracy, leading to a unique measurement of the masses of the exoplanets (Nesvorný and Vokrouhlický 2014; Schmitt et al. 2014; Deck and Agol 2015; Linial et al. 2018).

As an example, consider a pair of planets with period ratio of $P_2/P_1 = 1.52$. This period ratio is close to 3:2 and thus is affected by this resonant term, giving a TTV period of $38P_1$ by Eq. 9. Figure 2 compares two planets with this period ratio with zero eccentricity and mass ratios of 10^{-6} to a pair of planets with eccentricities of $e_1 = e_2 = 0.04$ and mass ratios near 10^{-7} . Both pairs of planets give nearly identical amplitudes for the large resonant term due to the masseccentricity degeneracy discussed above, while the larger mass ratio planets show a much stronger chopping variation. In this case, there is a clear difference between the TTVs of the two simulated systems: the inner planet shows a drift over three orbital periods, and a sudden jump every third orbital period, while the outer one shows a similar pattern over two orbital periods. In this example, the phase of the orbital parameters is set such that the TTV amplitudes match; change in the phase can also be indicative of a nonzero eccentricity contributing to the TTVs, and with an ensemble of planets which are believed to have a similar eccentricity distribution, the mass-eccentricity degeneracy may be broken statistically (Lithwick et al. 2012; Hadden and Lithwick 2014).

Transit Duration Variations

TDVs have given useful results for characterization of individual systems, though fewer in number than TTVs. Three mechanisms for TDV have been observed in planetary system orbiting a single primary star.

The first is torque due to the rotational oblateness of the star. It is a convincing model for the duration changes in Kepler-13 b (KOI 13.01 Szabó et al. 2012) and a controversial explanation for transit shape anomalies in PTFO 8-8695 (Barnes et al. 2013).

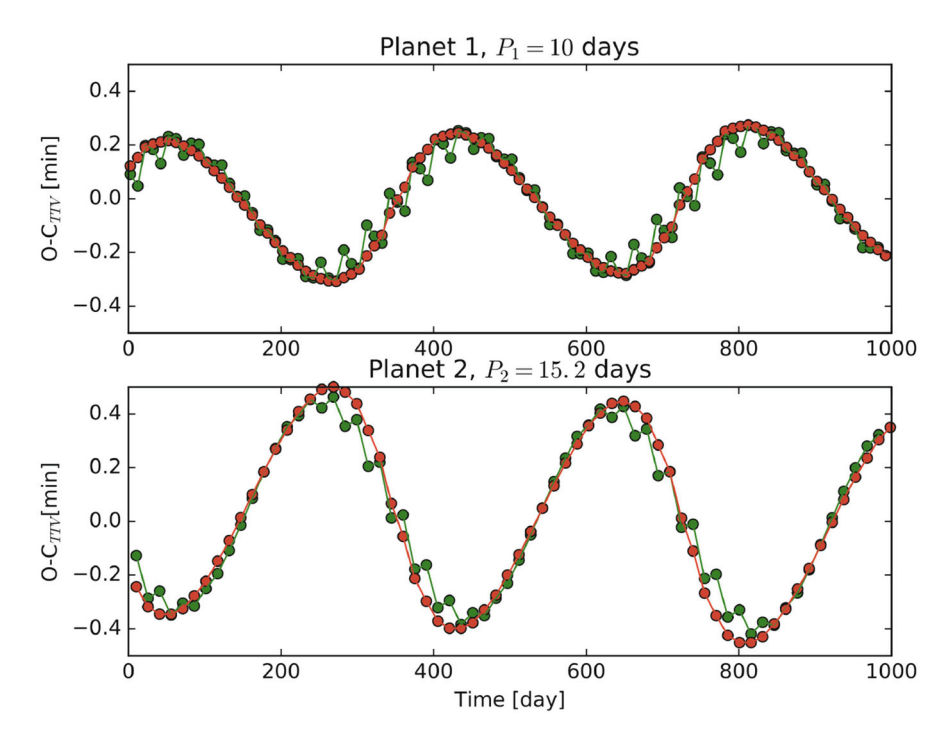


Fig. 2 Transit timing variations of two low-eccentricity planets with larger mass ratios, $m_1 = m_2 = 10^{-6} m_*$ (green) compared with two higher-eccentricity planets ($e_1 = e_2 = 0.04$) with smaller mass ratios $m_1 = m_2 = 10^{-7} m_*$ (red). The zigzag chopping component is apparent in the high-mass/low-eccentricity case while less apparent in the low-mass/high-eccentricity case

The second planetary cause of TDVs is eccentricity variations due to a resonant interaction. The length of the chord across the star and the speed at which the planet moves along that chord are changed during the planetary interaction. This effect has been observed in KOI-142 (Nesvorný et al. 2013). Slow, secular precession of the eccentricity is expected by general relativity (Pál and Kocsis 2008), by stellar oblateness (Heyl and Gladman 2007), and by tidal distortion (Ragozzine and Wolf 2009), but these mechanisms have not given rise to observable TDV to date, for planets around single stars. It is likely that very long time-baseline measurements, or comparing the measurements of two time-separated space missions like Kepler and Plato, will be able to detect this effect.

The third cause of TDVs for planets around single stars is inclination changes due to secular precession of the orbital plane. Torques from other planets were observed in Kepler-117 (Almenara et al. 2015) and Kepler-108 (Mills and Fabrycky 2017), the latter indicating mutual inclination of \sim 24° in a rather hierarchical pair of planets. A more dramatic example is that of KOI-120.01, which went from fully transiting to no eclipses at all during the Kepler mission; Judkovsky et al. (2020) interpret it as

a short-period planet perturbed by a few-AU binary companion. Similar phenomena in TOI-216b enabled a better radius measurement to reveal low bulk density for that planet (McKee and Montet 2023).

Earlier the case of Kepler-46 was described, in which TTV measurements of a transiting planet led to two degenerate possibilities for the identity of an additional, non-transiting, planet. The clever resolution (Nesvorný et al. 2012) was to note that in one of those solutions, to get the relative amplitudes of the component sinusoids correct in the TTV signal, the perturbing planet must be somewhat inclined with respect to the transiting planet. As a consequence, a torque on that planet would drive TDV. No such TDV were observed, so the unique solution – which is at a different orbital period and planetary mass, and closer to coplanar – was found.

Extending this inclination mechanism of TDV to two stars and a planet, the precession of circumbinary planets (CBPs) has been so extreme as to cause transits to turn on and off (Martin 2017). This observation is similar to the several known cases of stellar triples with inner sometimes-eclipsing binaries, but in this case, it is most observable in the outer orbit. The first case of that phenomenon was Kepler-35 (Welsh et al. 2012) and the most spectacular observed so far is Kepler-413 (Kostov et al. 2014), in which a 4° mutual inclination caused transits to stop and then start again nearly half a precession cycle later. More recently, the first circumbinary planet system with three transiting planets was found with the discovery of Kepler-47d, whose depth grew with time, thanks to the changing impact parameter (Orosz et al. 2019).

Additional dramatic TDVs can occur in CBP systems due to the moving-target effect described above for TTVs. If the transit occurs while the star is moving in the same direction as the planet, the transit duration is longer; if in opposite directions, the transit duration is shorter. Matching the prediction from the phase of the binary completely secures the interpretation of the signal that an object is in a circumbinary orbit, as discussed extensively by Kostov et al. (2013) for the cases of Kepler-47 and Kepler-64 (aka PH-1, KIC 4862625b).

As part of the TTV catalog of all the Kepler long-cadence data, Holczer et al. (2016) measured TDVs for the planets with large enough S/N, and Shahaf et al. (2021) described its statistical properties, finding 15 with significant secular trends. They also showed that statistically, the longer-period planets must have more massive or more inclined companions planets in comparison to the closer-in ones. Millholland et al. (2021) also analyzed these data, with conclusions described below.

Observational Considerations: Timing Precision

Transit light curves are constructed from a series of exposures, each yielding a flux measurement with an accompanying uncertainty. The dip in stellar flux during a transit causes a deficit of detected photons relative to the baseline flux outside of transit; this deficit is fit with a transit model which computes the loss of light caused

by the overlapping disks of the planet and star as a function of time. So, how does this sequence of flux measurements translate into a time of transit? And how do the uncertainties in flux translate into an uncertainty in the time of transit? The transit time is determined from the midpoint of a transit model which best fits the flux time series. The timing uncertainty is determined by how much the model can be shifted back and forth in time without degrading the fit significantly. Thus, the timing precision is primarily controlled by the steepest portions of a transit, which are the ingress and egress when the planet crosses onto and off of the disk of the star, causing a dip of depth $\delta = (R_p/R_*)^2$ if limb darkening is ignored. Suppose for the moment that the only source of noise is Poisson noise due to the count rate of the star, \dot{N} . The photometric uncertainty over the duration of ingress, τ (Eq. 3), scales as $(\dot{N}\tau)^{1/2}$. If the time of ingress fit from a model is offset by σ_{τ} , then the difference in counts observed versus the model is $\sigma_{\tau}\delta\dot{N}$ (the pink region in Fig. 3). Equating this count deficit to the photometric uncertainty gives

$$\sigma_{\tau} = \tau^{1/2} \dot{N}^{-1/2} \delta^{-1},\tag{10}$$

which is the 68.3% confidence timing precision assuming that the exposure time is much shorter than the ingress duration and that $\sigma_{\tau} \ll \tau$. The same formula applies to egress. A longer transit ingress duration leads to a shallower slope in ingress, which makes it more difficult to measure an offset in time of the model. Higher count rates and deeper transits improve the precision, as expected. Note that it has been assumed that the duration of the transit is sufficiently long that the error on δ is small.

Suppose the transit duration is T. Then, the uncertainty on the duration is given by the sum of the uncertainties on the ingress and egress, added in quadrature: $\sigma_T = \sqrt{2}\sigma_\tau$. The timing precision, σ_t , is set by the mean of the ingress and egress, giving $\sigma_t = \frac{1}{\sqrt{2}}\sigma_\tau$.

A more complete derivation of these expressions is given by Carter et al. (2008), while an expression which includes the effects of a finite integration time is given by Price and Rogers (2014). The assumptions of no limb darkening and Poisson noise are generally broken by stars; in addition, stellar variability contributes to timing uncertainty, for which there is yet to be a general expression. These effects generally increase the uncertainty on the measurement of transit times and durations,

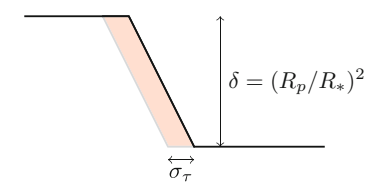


Fig. 3 Diagram of the transit ingress of a planet, flux versus time. The precision of the timing of ingress, σ_{τ} , is set by when the area of the ingress (pink) equals the timing precision over the duration of ingress. The same applies to egress, albeit with the time flipped in this plot

and so, the best practice would be to estimate the timing uncertainties from the data, accounting for effects of correlated stellar variability by including the full covariance matrix of the timing uncertainty (Carter and Winn 2009; Gibson et al. 2012; Foreman-Mackey et al. 2017). Crossing of the path of the planet across star spots may also cause some uncertainty on the timing precision (Oshagh et al. 2013; Barros et al. 2013); this can be diagnosed by a larger scatter within transit than outside transit or other signs of significant stellar activity and can be handled best by including the spots in the transit model (Ioannidis et al. 2016).

Note that the barycentric light-travel time offset must be carefully corrected for high-precision TTV (Fabrycky 2010; Eastman et al. 2010).

In some cases, the timing variations can be sufficiently large that the search for transits is impaired as standard algorithms (such as boxed least squares Kovács et al. 2002) assume a linear ephemeris (García-Melendo and López-Morales 2011). An early example of this was the planet Kepler-36b which was strongly perturbed by a close companion. Each transit was low signal to noise, and the Kepler pipeline initially missed this planet, thanks to the nonlinear ephemeris. A quasiperiodic pulse detection algorithm ("QATS") was adapted to search for nonlinear transits and identified this planet before the Kepler pipeline later identified the planet with a larger dataset (Carter and Agol 2013). This pair of planets was then precisely characterized, thanks to the proximity to 6:7 period ratio (Carter et al. 2012). Other algorithms have been developed to search for nonlinear ephemerides, most recently using a machine learning approach ("RIVERS" Leleu et al. 2021, 2022, 2023).

Science Results

Initial papers on TTVs were focused on the detection of additional planets in transiting planetary systems. This was borne out with the detections of Kepler-19 c and Kepler-46 c, as discussed above (Ballard et al. 2011; Nesvorný et al. 2012). However, the number of TTV detections is still modest (Christiansen 2022), with only 32 confirmed planet detections as of October 2024 according to the NASA Exoplanet Archive (NASA Exoplanet Science Institute 2020). A more productive application of TTVs has been toward measuring the masses of multi-transiting planetary systems.

One of the greatest challenges in the field of exoplanets is the measurement of the masses of earthlike exoplanets. This typically relies on measuring the Doppler reflex motion of a star, which becomes prohibitive for an earth-sun exo-twin: the best radial velocity amplitude precisions to date are typically $10-20\,\mathrm{cm/s}$, while the sun's radial velocity due to earth is $\approx 9\,\mathrm{cm/s}$. Improvements in RV precision have run into a noise floor caused by stellar variability and inhomogeneity; a path to breaking through this noise floor may be difficult, or impossible, to realize.

Alternatively, TTVs provide another path toward measuring the masses of earthlike exoplanets. However, there are two drawbacks for using the TTV method to measure planets' masses: (1) it requires transiting planet(s); (2) it requires the planets to be in close enough proximity that the TTVs exceed the timing noise.

Both RV and TTV can benefit if one can stretch the definition of "earthlike" to include host stars of smaller mass and size: the smaller stellar mass causes larger reflex motions of the star and timing variations the planets, which increases the amplitude of the RV and TTV signals. If the meaning of "earthlike" also includes locating the planet in the habitable zone, then low-mass stars have the additional advantage of a closer habitable zone, corresponding to a larger RV signal and a much higher probability of transit. In addition, a smaller star leads to a larger transit depth, which yields more precise transit times (Eq. 10).

Based on these considerations, the discovery of TRAPPIST-1 was a welcome addition to the family of multi-transiting planetary systems (Gillon et al. 2016). Eventually, seven planets were found to transit the star (Gillon et al. 2017; Luger et al. 2017), and the close proximity of their orbits and the small mass and radius of the host star made these promising for characterization of the planets with TTVs over several years of observation (Grimm et al. 2018; Agol et al. 2021a). In fact, these planets' masses can be characterized so precisely with TTVs that the RV technique may never match the precision, and for some of the planets, the mass precision is limited by the precision with which one knows the host star's mass. As discussed above, the transit depths and TTVs give model-independent bulk densities of the planets (but possibly still corrupted by the inhomogeneous brightness of the star). These density measurements yield a surprising result: the planets appear to be consistent with sharing a common composition, but their compositions differ from the solar system's terrestrial planets (see "► TRAPPIST-1 and Its Compact System of Temperate Rocky Planets" and Fig. 4). If the planets have a smaller ratio of core to mantle mass compared to earth, then their common compositions might be attributable to a deficit of iron relative to magnesium and silicon of the host star and birth planetary nebula relative to the sun. Unfortunately, astronomers have yet to measure the abundances of these refractory elements in the composition of the host star, and this interpretation is not unique.

Nevertheless, it is remarkable that in the TRAPPIST-1 case, one can even address these questions of terrestrial composition, thanks to the exquisite precision of the TTVs. For planet e, which is perhaps the most similar to earth, the measured mass precision would require a 2 millimeter-per-second radial velocity uncertainty to achieve the same precision for a planet at 1 AU around a solar twin. This is about two orders of magnitude more precise than the best current RV measurements, which exemplifies to the sensitivity of the transit timing technique when the right conditions are present.

A widespread phenomenon was detected by TTV characterization of masses: the existence of puffy sub-Neptune planets ("super-puffs"). In the first such case, Kepler-11 e (Lissauer et al. 2011), a planet whose mass is half Neptune's but whose radius is slightly bigger than Neptune's radius. Even more extreme cases of this class have been found, such as the $2.1^{+1.5}_{-0.8}M_{\oplus}$ planet with a radius of $7R_{\oplus}$ in Kepler-51b (Masuda 2014). These voluminous envelopes mean these low-mass planets formed while gas was still present in the protoplanetary disk and that they were able to capture that gas, a surprising result (e.g., Lee and Chiang 2016; Ginzburg et al.

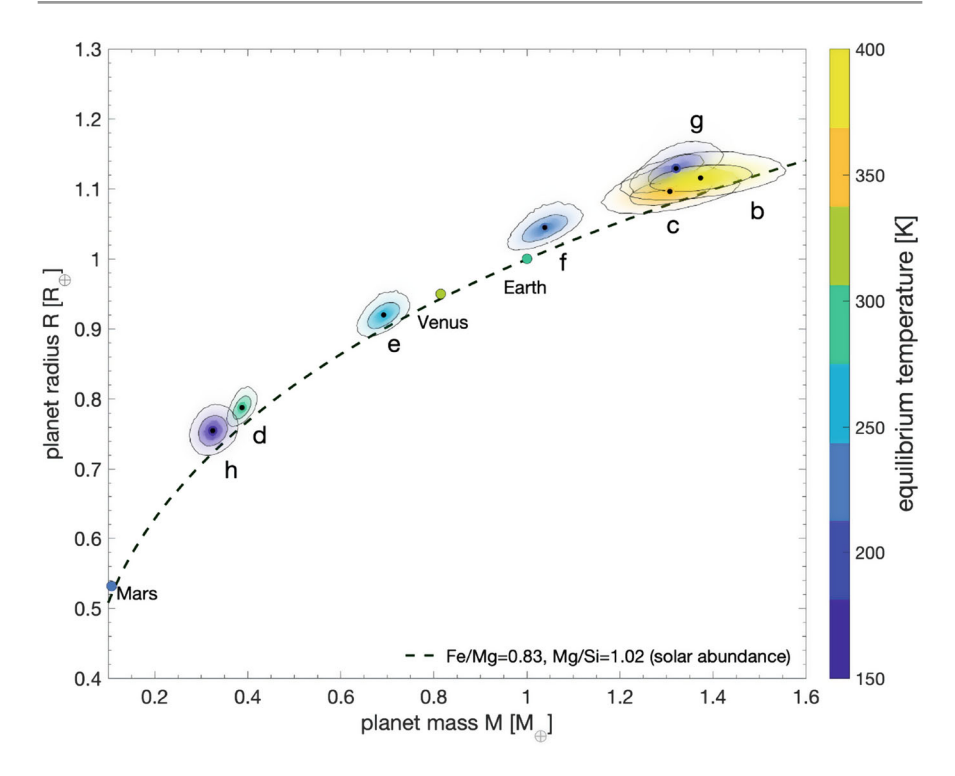


Fig. 4 Mass-radius relation of the TRAPPIST-1 planets based on Agol et al. (2021a)

2016). Alternatively, dusty outflows, high altitude haze, or heating by obliquity tides may be able to explain the large apparent sizes of these planets (Wang and Dai 2019; Gao and Zhang 2020; Millholland 2019).

Catalogs of transit times have been produced for the multi-planet *Kepler* systems (Mazeh et al. 2013; Rowe et al. 2015; Holczer et al. 2016; Ofir et al. 2018; Thompson et al. 2018; Lissauer et al. 2024). Several analyses of an ensemble of TTV pairs of planets have recently been carried out (Hadden and Lithwick 2014; Xie 2013, 2014; Jontof-Hutter et al. 2016; Judkovsky et al. 2022b, 2024; Ofir et al. 2025), with the largest by Hadden and Lithwick (2016), yielding constraints on the RMS eccentricity of the population of planets. At periods near \approx 10 days, the RV and TTV densities agree rather well. At shorter period, most of the RV detections are single planets, which in general appear to have lower density relative to their multi-planet counterparts (Steffen 2016; Mills and Mazeh 2017).

With the end of the primary *Kepler* mission, the data volume of transit times diminished until the launch of TESS. And yet analyses of Kepler data continue to provide new results. Millholland et al. (2021) used TDVs to argue that the so-called Kepler dichotomy, which is the observation from transiting planetary systems that the geometrical bias applied to statistical models of the multiple-planet systems

falls short of explaining all the single-transiting planets (Johansen et al. 2012), arguing for a model of two populations (Ballard and Johnson 2016), may instead be explained by a single population in which there is an anticorrelation between multiplicity and mutual inclination of planets; this is also confirmed with TTV analyses of the population, indicating that 30% of stars have planetary systems like those found with Kepler (Zhu et al. 2018). Yee et al. (2021) show that the Kepler systems analyzed with TTVs show eccentricities which are smaller than they would be if the systems were randomly drawn from the stable phase space, indicating that some sort of damping occurs; also see Van Eylen and Albrecht (2015) and van Eylen et al. (2019). Judkovsky et al. (2022b) show that photodynamical models can detect variations in the impact parameter of Kepler planets, which manifest as TDVs, caused by companion planets or other effects. Ofir et al. (2025) applied an analytic model to analyze more than 200 planets from the Kepler mission with photodynamics. A search for TTVs of hot Jupiters in the Kepler data reveals that some of these systems may have close companions (Wu et al. 2023). In addition, various systems have been subject to joint reanalysis with additional transit data from the full Kepler dataset and/or combined analyses with follow-up RV and/or transit observations (von Essen et al. 2018; Freudenthal et al. 2018, 2019; Saad-Olivera et al. 2017, 2018; Sun et al. 2019, 2022; Jackson et al. 2019; Masuda and Tamayo 2020; Petit et al. 2020; Vissapragada et al. 2020; Weiss et al. 2020; Liang et al. 2021; MacDonald et al. 2021, 2022; Greklek-McKeon et al. 2023). The Kepler dataset is a gift that keeps on giving for timing analyses.

After completion of the Kepler mission, the K2 mission continued to provide TTV systems, such as WASP-47, the first short-period hot Jupiter with nearby planet companions (Becker et al. 2015), as well as multi-planet systems K2-138 (Vivien et al. 2024), K2-146 (Hamann et al. 2019), and K2-24 (Nascimbeni et al. 2024; Teyssandier and Libert 2020). With the end of the K2 mission and launch of TESS in 2018 (Ricker et al. 2015), astronomers are presently in a new era of studying transit timing with the brightest stars on the sky which are also amenable to radial velocity follow-up. These observations are being accompanied by novel theoretical developments, described next.

Recent Theoretical Developments

Modeling of dynamically interacting planetary systems has continued to progress since the first version of this review. This includes algorithms for the detection of TTVs, characterization of systems with TTVs/TDVs, and interpretation of the dynamics of known dynamically interacting systems.

Ofir et al. (2018) developed a spectral approach to detecting TTVs for pairs of interacting planets, which they then applied to the Kepler dataset, resulting in a significant increase in the number of TTV detections.

As mentioned above, Leleu et al. (2021) developed a new machine learning approach to detecting transiting planets which display large TTVs and applied it to

Kepler data to detect new planets (Leleu et al. 2021, 2022). This method also reveals a possible bias when carrying out transit timing analyses due to underestimating the TTVs (Leleu et al. 2023).

Bayesian sampling of the dynamical parameters of transiting planetary systems can be improved with faster N-body algorithms. A symplectic approach was taken by Deck et al. (2014, "TTVFast"), which was given a Python interface by Canul et al. (2021, "nauyaca"). Other numerical codes for analyzing TTVs have been developed, such as Borsato et al. (2014, "TRADES") based on a Runge-Kutta integrator.

An open-source code based on perturbation theory was provided by Agol and Deck (2016, "TTVFaster"). An approximate semi-analytic approach was taken by Linial et al. (2018) who decompose the TTVs of a pair of planets into three "modes," after which a linear fit can yield the planets' masses, based on the insights of Lithwick et al. (2012). Hadden (2019) developed an analytic model for computing TTVs, "TTV2Fast2Furious," while Hadden and Tamayo (2022) give an example of computing TTVs with their Python code for perturbation theory, "celmech."

Photodynamical models enable more precise characterization of planets with shallow transits, such as Kepler-36 (Carter et al. 2012), and can yield more precise masses and densities. An analytic photodynamical model was developed and applied by Yoffe et al. (2021) and Judkovsky et al. (2022a,b, 2024), yielding more precise masses, radii, and densities (Judkovsky et al. 2023). In systems with extreme TDVs, including disappearing transits, a fast analytic model has been developed to characterize the dynamics by Judkovsky et al. (2020). These analytic models can be useful, but they are always approximate and will become inaccurate in certain parts of parameter space, at which point one needs to rely on N-body computation.

In systems with many planets, the high dimensionality of the model parameter space can prohibit standard Markov chain Monte Carlo techniques from converging quickly to the posterior probability. In addition, the optimization of models can be inhibited by inaccurate finite difference derivatives, which are also slow to compute (Rein and Tamayo 2016). Thus, the accurate computation of derivatives of transittimes with respect to initial conditions can greatly improve the computation of the maximum likelihood and likelihood profile and improve posterior probability sampling using Hamiltonian/hybrid Monte Carlo (HMC) (Duane et al. 1987) and/or the No U-turn Sampler (Hoffman et al. 2014, "NUTS"). The first transit timing code to implement derivatives analytically was developed in the Julia language for speed and ease of use (Agol et al. 2021b, "NbodyGradient.jl"). This code made possible the sampling of the TRAPPIST-1 system in a small amount of CPU time (Agol et al. 2021a). More recently, Kento Masuda has developed a symplectic transit timing model based on automatic differentiation (Baydin et al. 2018) in the JAX language (Dai et al. 2023; Jones et al. 2024; Masuda et al. 2024, "jnkepler"). Differentiable photodynamical models have also been developed as part of inkepler (in JAX) and in Julia (Langford and Agol 2024, "Photodynamics.jl"). The JAX (Bradbury et al. 2018) and Julia (Bezanson et al. 2017) languages provide user interfaces which are interactive and high level but also use just-in-time compiling to provide code which

runs fast, solving the "two-language" problem. These codes will help to improve statistical analyses of the parameters of dynamically interacting planetary systems.

Once a system is analyzed, its dynamical state can be characterized. MacDonald et al. (2023) developed a code "exoMMR" for diagnosing the possible presence of mean-motion resonances, and they also forecast the expected TTV amplitudes for systems with detected resonances. Several papers have examined the statistics of period ratios and TTV "phase" in pairs of Kepler planets (Goldberg and Batygin 2023; Choksi and Chiang 2023; Wu et al. 2024; Li et al. 2024). These papers propose that the TTV phase, caused by nonzero free eccentricity, may be excited by a variety of mechanisms: secular forcing by more distant companions, turbulence in the protoplanetary disk, scattering by small bodies, or giant impacts. None of these theories yet provides a perfect match to the data, but some make predictions that may be tested with further examination of the dynamical states of these systems.

Delisle et al. (2017) have shown that TTVs may be used to probe planetary spin dynamics, while Boley et al. (2020) showed that the shortest timescale eigenfrequency can determine the rate of change of TDVs, which can cause some transits to (dis-)appear with time.

Extreme TTVs/TDVs can occur for binary planets in which two planets orbit about their center of mass, which in turn orbits about the star. This leads to large timing and duration variations, as modelled by Chakraborty and Kipping (2022) and Martin et al. (2019).

These theoretical developments will help to address a new era of TTV/TDV analysis being ushered in by TESS, described next.

Transit Timing in the TESS Era

The TESS mission is currently in operation, with each sector covered for about one sidereal lunar month at a time, while the polar caps are covered for up to one year of contiguous sectors (Ricker et al. 2014). Despite the short duration of each sector relative to Kepler, this mission has discovered planets transiting some of the brightest stars on the sky, making these stars amenable to transit timing follow-up with ground-based telescopes and other space-based telescopes, such as CHEOPS (Fortier et al. 2014; Borsato et al. 2021b). Despite its smaller aperture, TESS has been able to detect transits for some Kepler planet systems, extending the time baseline significantly (Jontof-Hutter et al. 2021, 2022; Battley et al. 2021; Yahalomi et al. 2023). The longer duration of observations at the polar caps and the multiyear coverage as TESS alternates between the Southern and Northern hemispheres enables the longer-term monitoring necessary for TTV analyses, which was anticipated by Hadden et al. (2019). This has made TESS a prolific telescope for the discovery and characterization of systems displaying TTVs. Here, a number recent discoveries are highlighted.

Examples of pairs of transiting planets which are in mean-motion resonance are rare, yet TESS provided an early example with the pair of planets TOI-216b/c (Kipping et al. 2019; Dawson et al. 2019, 2021; Nesvorný et al. 2022). The inner

planet was initially grazing, preventing a measurement of the planet's radius, but with further observations, the planet is now fully transiting the disk of the star, revealing the planet's radius, which implies a low density; this is an extreme example of TDVs (McKee and Montet 2023). A non-transiting companion planet was detected from large transit timing variations of transiting planet TOI-2015b (Jones et al. 2024), but as with Kepler-19c, the period of the perturbing planet is ambiguous. Another planet detected with TTVs by TESS is TOI-199c (Hobson et al. 2023), which may reside in its star's habitable zone. Other systems display TTVs for larger transiting planets, including TOI-2525 (Trifonov et al. 2023), TOI-2202 (Trifonov et al. 2021; Rice et al. 2023), TOI-1803 (Zingales et al. 2025), and TOI-5404b (Vítková et al. 2025); the latter planet shows the largest TTVs of any planet to date with variations of ± 2 days!

Resonant chains are rare but treasured for helping to constrain formation and migration processes in high-multiplicity planetary systems. TESS found several sixplanet systems with some or all of the planets in a resonant chain: TOI-1136 is a system of six transiting exoplanets (Dai et al. 2023); TOI-178 also contains six planets, of which the outer five appear to be in a resonant chain (Leleu et al. 2021, 2024b; Delrez et al. 2023); and HD 110067 (Luque et al. 2023) has all six planets in a resonant chain (Lammers and Winn 2024).

Other TESS systems do not reside in resonant chains but do display TTVs which have been employed to constrain the planet masses and orbits, such as TOI-270 (Kaye et al. 2021), TOI-1246 (Turtelboom et al. 2022), and TOI-1130 (Huang et al. 2020; Borsato et al. 2024). The system TOI-1130 consists of a hot Jupiter ("c") with an interior Neptune-mass planet ("b"), both with percent precision on their masses and radii; a transit of planet b was missed in followup observations, indicating the presence of large TTVs induced by the outer companion, confirmed by later observations which showed large TTVs, enabling a photodynamical characterization of the system (Korth et al. 2023; Borsato et al. 2024). Two of the planets in the TOI-2076 system show anticorrelated TTVs but which do not yet enable a precise mass constraint (Osborn et al. 2022). The planet TOI-2818b shows TTVs but does not yet have sufficient data to determine the nature of the companion, while RV upper limits rule out some TTV solutions (McKee et al. 2025). TOI-1749 shows hints of TTVs in the outer two planets (Fukui et al. 2021), without sufficient data to make a clear TTV characterization. Most recently, TTVs have been detected for planets transiting a star which is visible to the human eye (Bonfanti et al. 2025). Some systems are expected to show detectable TTVs but lack sufficient observations, such as TOI-125 (Quinn et al. 2019), TOI-561 (Lacedelli et al. 2020; Weiss et al. 2021), TIC 279401253 (Bozhilov et al. 2023), TOI-2096 (Pozuelos et al. 2023), HD 152843 (Nicholson et al. 2024), and TOI-700 (Gilbert et al. 2020, 2023). The latter system is remarkable in that it hosts two earth-sized planets close to a 4:3 period ratio in the host M-dwarf star's habitable zone. The system LP 791-18 has a host star which is bright enough for follow-up transit timing observations with ground-based telescopes, which yield a mass of the temperate Earth-sized planet in the system and constrains its tidal heating rate (Peterson et al. 2023). In the case of TOI-1266, Cloutier et al. (2023) used the mass measurements from RV and the *lack* of TTV to place a more stringent upper limit on the eccentricities of the two inner planets than the limit placed by RV.

With its all-sky coverage, TESS has provided access to younger transiting planetary systems, such as AU Microscopi, which contains an edge-on circumstellar disk and has been followed up with transit timing measurements using CHEOPS (Plavchan et al. 2020; Wittrock et al. 2022, 2023; Martioli et al. 2021; Szabó et al. 2021, 2022). HIP 41378 f shows a long-term quadratic trend in the transit times, which likely needs more data to derive a dynamic solution (Bryant et al. 2021; Alam et al. 2022). The young planet TOI-1227 b shows a long-term timing trend (Almenara et al. 2024). Each of these systems offers the prospect of characterization of the masses of these planets with both radial velocity and transit timing, which has a significant advantage of being able to check that both techniques agree, instead of being confused by stellar variability or other systematics (see below).

What can one learn from these systems? TESS has given stronger evidence that multi-planet systems have evolved dynamically over time. Younger systems appear to have a higher incidence of pristine resonances (Dai et al. 2024), while the period ratios of older systems can be modeled with a mix of resonances and broken resonances caused by planetary collisions (Li et al. 2024). Since the sizes of planets evolve with time, either due to cooling or envelope loss, the masses of planets are needed to diagnose the evolution over time, which TTV can provide in the case of closely spaced multi-transiting planetary systems. The early evolution of systems due to planetary migration can even be constrained with the architecture of these systems. In TOI-1136, the proximity of two of these planets to a 7:5 period ratio informs the system's migration history due to the delicate nature of second-order resonances (Dai et al. 2023).

Early work on transit timing carried out searches for companions of hot Jupiters, many of which turned up empty-handed (Steffen et al. 2012b); TESS seems to confirm this (Zhang et al. 2024). Gradually, companions to hot Jupiters were found with Kepler and K2 (Wu et al. 2023), and now, the TESS spacecraft has found its first examples of interior companions to hot Jupiters, TOI-1130b/c (mentioned above) and TOI-1408b/c (Korth et al. 2024). The Jupiter-sized planet TOI-1408b shows grazing transits with a period of 4.4 days, which was found by the standard TESS pipeline. The second planet was missed by the TESS pipeline and later found to transit with custom pipelines, due to its much smaller size and due to the largest fractional TTVs of any system found to date. The presence of nearby companions to hot Jupiters places strong constraints on models of their formation and migration (Dawson and Johnson 2018).

Transit Timing Versus Radial Velocity

The transit timing and radial velocity techniques can both suffer from systematic errors which can make the inferred masses incorrect. The most common errors are due to additional planets or stellar activity noise, but other issues can affect either technique, such as complications with the instrument, data incompleteness, analysis, and/or modeling inaccuracies. Thus, a cross-comparison between these techniques can help to bolster our confidence in both techniques. Such a comparison has been limited but may be about to grow significantly with the advent of the TESS mission.

With the Kepler mission came the first detections and growth of the transit timing technique for measuring masses of exoplanets. However, the Kepler field covers a small part of the sky with few stars which allow for measurement of their planetary masses with radial velocity. Radial velocity surveys instead target the brightest stars across the sky to achieve smaller photon noise, as well as to better characterize the stellar jitter using spectral diagnostics. Thus, in the Kepler era, there were only a handful of planets with both transit timing mass measurements *and* radial velocity measurements, allowing for limited comparison of the two techniques.

Sample-level comparisons between RV and TTVs circumvented the incompatibility of Kepler and RV surveys (e.g., Wolfgang and Laughlin 2012; Zeng et al. 2019), but selection effects can plague these comparisons (Steffen 2016; Mills and Mazeh 2017; Jontof-Hutter 2019; Otegi et al. 2020; Zhu 2020), and overcoming these biases requires careful correction (Leleu et al. 2023, 2024a). Since the TESS spacecraft is now covering the brightest stars on the entire sky, transiting planet hosts can now be characterized with radial velocity measurements (as well as with astrometry and direct imaging). Since transits have a low probability, transiting planet hosts are typically fainter than host stars of radial velocity surveys. However, with the advent of the ESPRESSO instrument on the VLT (Pepe et al. 2021), high-precision RV is now possible with many transiting planet host stars. The CARMENES instrument on Calar Alto 3.5-meter observatory (Quirrenbach et al. 2014) is also extending high-precision RV measurements to M dwarf stars, which are also fainter but are better represented in the TESS sample than in the Kepler sample.

Direct comparisons of TTV and RV mass measurements are now available for a growing number of systems. Figure 5 shows a selection of planets taken from the literature for which the masses have been measured separately with TTVs and RV. There is a good correlation between the two methods; in some cases, one technique gives better precision than the other, but in general, the masses are consistent, which is good news for both techniques. One outlier is Kepler-89d/KOI 94.01 (Weiss et al. 2013; Masuda et al. 2013) in which the TTV mass is smaller by factor of ≈2 relative to the RV mass. This is system with four transiting planets, for which the best-fit TTV model is a poor fit. Jontof-Hutter et al. (2022) find a slightly larger mass, reducing the tension of the fit, but more work remains to determine if, perhaps, adding an additional planet to the system can produce a better TTV fit, agree with the RV data, and resolve the tension between the RV and TTV masses.

One way to contrast transit timing with radial velocity is to compute the equivalent radial velocity semi-amplitude uncertainty required to obtain the same mass uncertainty as a transit timing measurement. Based on data from the NASA Exoplanet Archive, the RV-equivalent precision was computed for TTV-measured

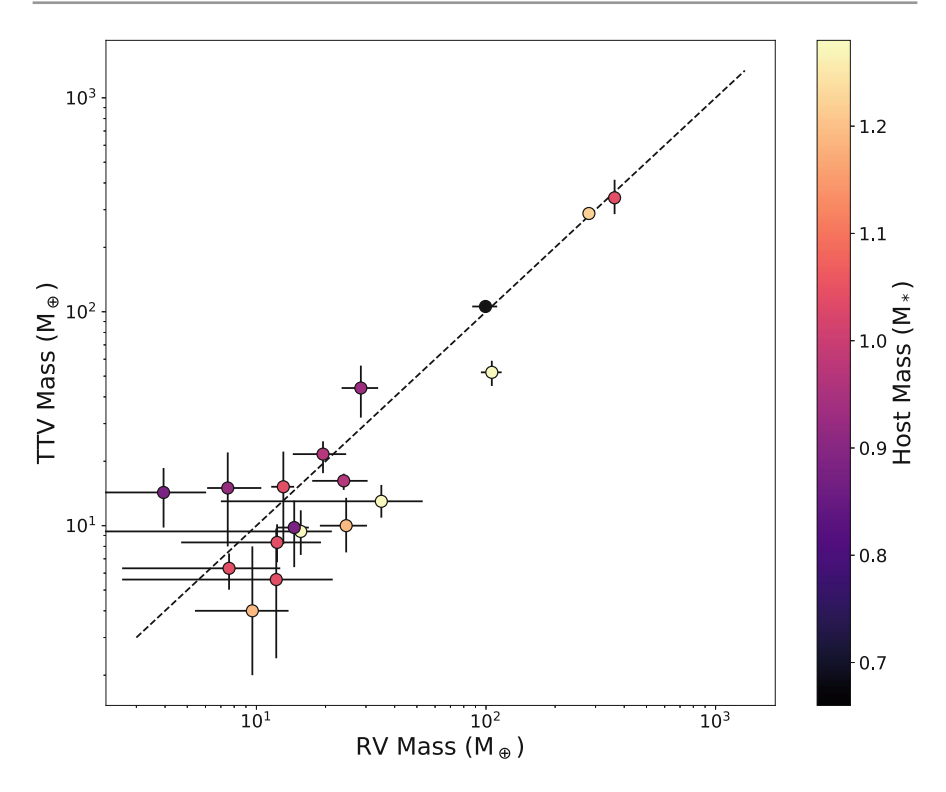


Fig. 5 Plot of measured masses of transiting exoplanets with TTV and RV measurements. (Figure credit: Tyler Gordon)

masses (some of these TTV masses may be limited by the measurement precision of the host star), as well as the RV-semi-amplitude precision for planets with masses measured with RV. After correcting several typos in the database and in published papers, Fig. 6 shows that radial velocity measurements have been improving versus year of publication. However, the highest equivalent precision of the two techniques is given by TTVs. A drawback for precision TTV mass measurements is that they require extensive observations, so no measurements better than 6 cm/sec equivalent have been published since 2021.

This figure may indicate that TTV could be used in the future as a calibrator of extreme-precision radial velocity (ePRV) measurements. As larger telescopes with better instrumentation continue to improve RV precision, the effects of stellar variability can dominate the noise, and detrending or mitigating these effects can be complicated. If TTV systems found around bright stars can be characterized with high precision, perhaps in the future these systems may be used to calibrate ePRV detrending techniques.

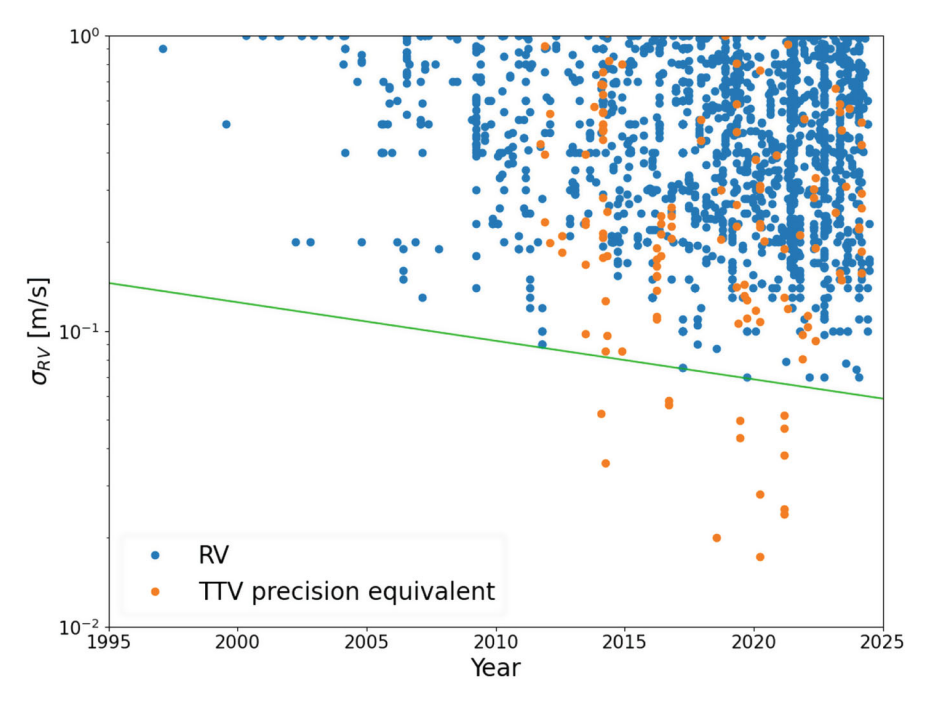


Fig. 6 Radial velocity semi-amplitude precision (blue) and semi-amplitude equivalent for TTV mass measurements (orange). Green line shows the improvement in RV precision with time. All of the highest precision measurements below 6 cm/s belong to the TTV technique

Transit Timing with HST and JWST

Much of the exoplanet focus of HST and JWST has been trained on the detection and characterization of exoplanet atmospheres, thanks to their photometric stability, near-infrared spectroscopic capability, and, for JWST, mid-infrared sensitivity (Beichman et al. 2014). Despite the power of HST and JWST, for many planets, the detection of an atmosphere cannot be accomplished in a single visit but must build up signal to noise with multiple transit and/or secondary eclipse measurements. For example, a significant portion of JWST time has been devoted to characterizing the atmospheres of the TRAPPIST-1 system planets with observations of multiple transits and secondary eclipses. The multiple visits to each of the planets in this system will provide transit times and durations, which will likely yield more precise constraints on the dynamical properties of the system than with the Spitzer telescope, thanks to the much larger collecting area and sensitivity to the peak of the star's SED. The secondary eclipses can provide a complementary constraint on the orbital eccentricities of the planets (Winn 2010; Heyl and Gladman 2007), which can potentially break TTV degeneracies.

Serendipity can also allow HST or JWST to detect TTVs. The HST transit of Kepler-1625b showed a significant timing offset relative to the Kepler ephemeris (Teachey and Kipping 2018), likely due to a planetary companion or, more intriguingly, potentially due to a candidate exomoon. The transits of the planets Kepler-51 b and d (Libby-Roberts et al. 2020; Masuda et al. 2024) show timing offsets with HST and JWST. A timing analysis implies that a fourth planet must be present in the system, while more data will be required to disentangle the nature of this system of low-density planets.

Another aspect of transit timing which can be probed with JWST is wavelength dependent times of transit. This effect was predicted by Dobbs-Dixon et al. (2012) for simulated hot Jupiter transit-transmission spectra. The offsets are not due to the dynamics of the orbital motion but instead are due to atmospheric dynamics. Stellar irradiation can drive a super-rotating circumplanetary jet, which causes the Eastern terminator to be hotter than the Western, causing a difference in scale heights along the two sides of the planet. The wavelength dependence of the opacity then causes the shadow of the planet to appear distorted and offset at some wavelengths, causing an artificial timing offset when the transits are fit with a circular planet shadow. This effect was detected for the first time with JWST by Rustamkulov et al. (2023) in the hot Jupiter WASP-39b, which displayed wavelength-dependent timing offsets which were qualitatively consistent with the predictions of Dobbs-Dixon et al. (2012).

A Prescription for Transit Timing/Duration Analyses

Here is a brief guide for transit timing and duration analyses. The first step involves measuring the times and durations of the individual transits. Usually, this requires fitting a transit light curve to the transits, often holding the radius ratio fixed, and allowing the transit time, duration, and impact parameter to vary, and then sampling these parameters from the posterior probability distribution. Many tools exist to carry out these analyses, as described in other chapters, such as EXOFASTv2, exoplanet, and jaxoplanet (Eastman et al. 2019; Foreman-Mackey et al. 2021; Hattori et al. 2024).

The next critical component of the analysis involves determining if there are detectable TTVs/TDVs. This requires confidence in the error bars and then seeing whether the times (durations) are consistent with a linear ephemeris (constant value). If the chi-square is large for these, then it could be indicative of the presence of TTVs/TDVs; it could also mean that the error bars are underestimated or that there are outliers present. Usually, a large number of measurements are necessary for redundancy in checking for outliers; in addition, a sufficiently long sampling timescale is needed for an accurate analysis. It is best to have a duration of two super-periods which is well sampled. If two planets are in close proximity and are close to a resonance, then the TTV amplitude can be estimated based on mass-radius relations and analytic formulae.

If one is confident of the detection of TTVs/TDVs and would like to characterize the system, then next a model for the timing must be developed. Analytic approaches

are much faster computationally and can be useful for an initial analysis, but they are approximate, so a full analysis should also be carried out with N-body integration. This usually involves integrating Newton's force laws with time and then finding the minimum projected sky separation to determine the mid-transit time (Fabrycky 2010). An example of computing TTVs is given in the open-source REBOUND N-body code GitHub repository (Rein and Liu 2012). An initial model must be found for the TTVs/TDVs, which is often a tricky prospect. If the period and/or amplitude of the TTVs/TDVs is revealed by Fourier analysis, then analytic estimates may be used to seed the dynamical model. Often, this means placing a perturber near a resonance to produce large sinusoidal TTVs (although if more than one planet transits, and companion planets are in close proximity, then this can make this step straightforward).

Next, the N-body model must be optimized. This typically involves computing a gradient of the likelihood with respect to the dynamical parameters, and often, finite differences are used for this purpose, although gradient-based computations have become available more recently, either analytic or with automatic differentiation (as discussed above). The Levenberg-Marquardt algorithm works well when the uncertainties are normal, while the Broyden-Fletcher-Goldfarb-Shanno algorithm (BFGS) tends to work well otherwise (Fletcher 1987). Other approaches involve gradient-free optimization, such as Nelder-Mead, or simply running a Markov chain and picking the highest likelihood, but these tend to be slower. With the optimized model, then one must ask again whether the model matches the data. Frequently, the chi-square is large (compared with the number of degrees of freedom), and so again, there exists several possibilities: perhaps, the optimum likelihood was not found; perhaps, the error bars are underestimated; perhaps, the dynamical model is inadequate (often this means another perturbing planet, which can be exciting); or perhaps, there are outliers in the data. The residuals can be examined, both temporally to look for correlated patterns which may indicate an inadequate model and examining the normalized residuals to see whether they look Gaussian or whether there may be outliers present. If correlations are not present, and the errors appear normal, but the standard deviation is too large, then often times rescaling of the uncertainties or adding a systematic noise error in quadrature to the measurement errors can suffice to account for a large reduced chi-square. Once the model is re-optimized with the scaled uncertainties, then the uncertainties on the model parameters can be estimated from the information matrix (note that this step assumes that the likelihood is a multidimensional Gaussian, which is often not the case, but it does supply a starting estimate for parameter errors). Although this has yet to be widely applied to timing analyses, a cross-validation approach is valuable if there is sufficient data, in which some data are excluded, the model is optimized to the remaining data, and then, the model is used to forecast the excluded data. This approach can be used to test how robust the model solution is and can possibly be used in flagging outliers or determining whether to introduce more complexity to the model. Prior to sampling the full probability, one should carry out a profile of the likelihood. This involves stepping through each parameter, holding it fixed, and optimizing the likelihood with respect to the remaining parameters. This can help to identify degeneracies in the model or help to find other modes of the likelihood (i.e., high-probability regions) which may not be sampled well by MCMC. The widths of the profile of each parameter may be compared with the information matrix error estimates to see whether these are comparable.

The penultimate step involves sampling the posterior probability of the model given the data. The sampling step is only meaningful if the physical model and the statistical model represent the data well, and so, care must be taken to address these issues. Techniques that are standard now are using Markov chain Monte Carlo or nested sampling; however, these methods can have difficulty converging in high-dimensional parameter spaces. Again, gradient-based algorithms can enhance convergence with HMC or NUTS. If the initial optimization revealed multiple solutions with similarly good fits, then sampling each of these "modes" is necessary before reporting uncertainties.

Finally, once the posterior parameters are derived, then a dynamical analysis can take place. Often, this involves examining the long-term stability of the system, measuring the free and forced eccentricities, looking for signs of resonance, etc. If an ensemble of systems is being studied, then a statistical examination of their properties can take place.

Unsolved Problems and Future Developments

Future work on TTVs and TDVs can continue to improve our application of these techniques and to better understand their planetary systems. One unsolved problem is the presence of excess timing noise in transit timing measurements. In some cases, the source(s) of this noise have not yet been identified and may be due to stellar variations (e.g., variability of the total flux due to granulation, spot crossings, and/or flares) or potentially due to systematics (either due to instrumental or atmospheric instability). This excess noise is apparent when comparing the excess timing scatter in single- and multi-transiting planetary systems in the Kepler dataset (Siegel and Rogers 2022). Robust statistics may be used to handle outliers, such as the Student's t-distribution (Jontof-Hutter et al. 2016; Agol et al. 2021a). Recent JWST observations of TRAPPIST-1 show an excess of low-amplitude stellar flares (Howard et al. 2023), which were below the threshold of detection in prior Spitzer and Kepler data, which may be a culprit for timing outliers.

Other future work could address theoretical modeling of transit timing. Analytic models for TTVs may underestimate the "chopping" component (Deck and Agol 2015). Searching for companion planets requires a global search through parameter space, which can be difficult, thanks to the narrow high-probability regions occupied by transit timing solutions in a high-dimensional parameter space. Several works have pointed out possible biases in TTV analyses, which is a problem which has yet to be fully explored. While analyzing transit timing variations, it is typical to consider long-term stability of the system after a posterior has been derived from the timing model (e.g., Deck et al. 2012, applied to Kepler-36). Incorporating stability

criteria directly into the timing analysis could help improve the dynamical characterization (e.g., Tamayo et al. 2020). Finally, distinguishing TTVs of companion planets from exomoons could use more theoretical investigation to improve ongoing searches for exomoons (Kipping 2020; Kipping and Teachey 2020; Kipping and Yahalomi 2022; Yahalomi et al. 2024). Machine learning and artificial intelligence has yet to be widely applied to transit timing and duration variations. Chen et al. (2024) have developed the "DeepTTV" model, while Ikhsan et al. (2024) have investigated the application of machine learning for the TTV inverse problem.

Continuing to search for and catalog transit timing and duration variations is an ongoing work. Kepler catalogs continue to be refined (Lissauer et al. 2024). There has yet to be a catalog for TESS, with the exception of Ivshina and Winn (2022) which only examines hot Jupiters, and finds that only WASP-12 shows evidence of period decay. Most transit timing studies are bespoke for each high-multiplicity system, as the analyses are detailed and tedious, and each system seems to contain a surprise or a puzzle. Streamlining, automating, and producing an assembly line for these analyses would be a valuable endeavor – perhaps a job for the next generation of AI?

This is especially important work as the collection of transit measurements will continue to grow throughout this decade and the next. The ARIEL space telescope will primarily be focused on spectroscopic characterization of transiting extrasolar planets (Tinetti et al. 2018). It will greatly improve on CHEOPS, thanks to its larger collecting area and its more placid orbit near L2 (Tinetti et al. 2016). It is due to launch in five years time and will operate for four years, allowing sufficient time for multiple visits of some transiting planets to improve on the signal to noise but also to simultaneously search for TTVs (Borsato et al. 2021a). The Roman mission (aka WFIRST/WFIRST-AFTA) will not be targeted, but it will revisit the same fields numerous times, with many transiting planet detections expected (Montet et al. 2017), enabling a search for TTVs and TDVs (Wang and Espinoza 2023).

The PLATO mission is due to launch in 2026 (Rauer et al. 2014), while the "Earth 2.0" mission is due to launch in 2028 (Ge et al. 2022); these may well cause another spike in TTV science. These missions have the prospect of detecting new planets in systems already characterized with Kepler and TESS, as well as extending the timing baseline significantly (Eschen et al. 2024). On a longer timescale, the Habitable Worlds Observatory may expand on the capabilities of JWST for precision transit spectroscopy (Gaudi et al. 2020), sometimes requiring multiple visits which can then be used for timing analyses. A concept being studied for a very large aperture set of space telescopes could greatly improve precision spectroscopy of transiting planet systems (Apai et al. 2019, "Nautilus"). This would help in overcoming the limits of stellar variability on transit characterization (Gordon et al. 2020), potentially enabling the future study of solar system analogues (Lindor and Agol 2024).

The future of characterizing multi-transiting planet systems with TTVs and TDVs looks promising.

Cross-References

- ▶ Detecting and Characterizing Exomoons and Exorings
- ▶ Dynamical Evolution of Planetary Systems
- ▶ Space Missions for Exoplanet Science: Kepler/K2
- ▶ Space Missions for Exoplanet Science: TESS
- ► The Way to Circumbinary Planets
- ► Tightly Packed Planetary Systems
- ▶ Tools for Transit and Radial Velocity Modelling and Analysis
- ► Transit Photometry as an Exoplanet Discovery Method
- ► TRAPPIST-1 and Its Compact System of Temperate Rocky Planets
- ▶ Two Suns in the Sky: The Kepler and Tess Circumbinary Planets

Acknowledgments E.A. acknowledges support from NSF grant AST-1907342, NASA NExSS grant No. 80NSSC18K0829, and NASA XRP grant 80NSSC21K1111. This work was completed, while D.C.F. was supported by (while serving at) National Science Foundation. Thanks to Dr. Tyler Gordon for compiling the data and creating Fig. 5.

Competing Interest Declaration The author(s) has no competing interests to declare that are relevant to the content of this manuscript.

References

Adams JC (1847) An explanation of the observed irregularities in the motion of Uranus, on the hypothesis of disturbances caused by a more distant planet; with a determination of the mass, orbit, and position of the disturbing body. MmRAS 16:427

Agol E, Deck K (2016) Transit timing to first order in eccentricity. ApJ 818:177

Agol E, Steffen J, Sari R, Clarkson W (2005) On detecting terrestrial planets with timing of giant planet transits. MNRAS 359:567–579

Agol E, Dorn C, Grimm SL et al (2021a) Refining the transit-timing and photometric analysis of TRAPPIST-1: masses, radii, densities, dynamics, and ephemerides. Planet Sci J 2(1):1

Agol E, Hernandez DM, Langford Z (2021b) A differentiable n-body code for transit timing and dynamical modelling—I. Algorithm and derivatives. MNRAS 507(2):1582–1605

Alam MK, Kirk J, Dressing CD et al (2022) The first near-infrared transmission spectrum of HIP 41378 f, a low-mass temperate Jovian world in a multiplanet system. ApJ 927(1):L5

Almenara JM, Díaz RF, Mardling R et al (2015) Absolute masses and radii determination in multiplanetary systems without stellar models. MNRAS 453:2644–2652

Almenara JM, Bonfils X, Guillot T et al (2024) Evidence for transit-timing variations of the 11 Myr exoplanet TOI-1227 b. A&A 683:A96

Apai D, Milster TD, Kim DW et al (2019) Nautilus observatory: a space telescope array based on very large aperture ultralight diffractive optical elements. In: Hallibert P, Hull TB, Kim DW (eds) Astronomical optics: design, manufacture, and test of space and ground systems II. SPIE, p 7

Ballard S, Johnson JA (2016) The Kepler dichotomy among the M dwarfs: half of systems contain five or more coplanar planets. ApJ 816(2):66

Ballard S, Fabrycky D, Fressin F et al (2011) The Kepler-19 system: a transiting $2.2~R_\oplus$ planet and a second planet detected via transit timing variations. ApJ 743:200

- Barnes JW, van Eyken JC, Jackson BK, Ciardi DR, Fortney JJ (2013) Measurement of spin-orbit misalignment and nodal precession for the planet around pre-main-sequence star PTFO 8-8695 from gravity darkening. ApJ 774:53
- Barros SCC, Boué G, Gibson NP et al (2013) Transit timing variations in WASP-10b induced by stellar activity. MNRAS 430:3032–3047
- Battley MP, Kunimoto M, Armstrong DJ, Pollacco D (2021) Revisiting the Kepler field with TESS: improved ephemerides using TESS 2-min data. MNRAS 503(3):4092–4104
- Baydin AG, Pearlmutter BA, Radul AA, Siskind JM (2018) Automatic differentiation in machine learning: a survey. J Mach Learn Res 18(153):1–43
- Becker JC, Vanderburg A, Adams FC, Rappaport SA, Schwengeler HM (2015) WASP-47: a hot Jupiter system with two additional planets discovered by K2. ApJ 812:L18
- Beichman C, Benneke B, Knutson H et al (2014) Observations of transiting exoplanets with the James Webb space telescope (JWST). PASP 126:1134–1173
- Berger TA, Huber D, Gaidos E, van Saders JL (2018) Revised radii of Kepler stars and planets using Gaia data release 2. ApJ 866(2):99
- Bezanson J, Edelman A, Karpinski S, Shah VB (2017) Julia: a fresh approach to numerical computing. SIAM review 59(1):65–98
- Boley AC, Van Laerhoven C, Granados Contreras AP (2020) Transit duration variations in multiplanet systems. AJ 159(5):207
- Bonfanti A, Amateis I, Gandolfi D et al (2025) Radii, masses, and transit-timing variations of the three-planet system orbiting the naked-eye star TOI-396. A&A 693:A90
- Borkovits T, Érdi B, Forgács-Dajka E, Kovács T (2003) On the detectability of long period perturbations in close hierarchical triple stellar systems. A&A 398:1091–1102
- Borkovits T, Csizmadia S, Forgács-Dajka E, Hegedüs T (2011) Transit timing variations in eccentric hierarchical triple exoplanetary systems. I. Perturbations on the time scale of the orbital period of the perturber. A&A 528:A53
- Borsato L, Marzari F, Nascimbeni V et al (2014) TRADES: a new software to derive orbital parameters from observed transit times and radial velocities. Revisiting Kepler-11 and Kepler-9. A&A 571:A38
- Borsato L, Nascimbeni V, Piotto G, Szabó G (2021a) Exploiting the transit timing capabilities of Ariel. Exp Astron 53(2):635–653
- Borsato L, Piotto G, Gandolfi D et al (2021b) Exploiting timing capabilities of the CHEOPS mission with warm-Jupiter planets. MNRAS 506(3):3810–3830
- Borsato L, Degen D, Leleu A et al (2024) Characterisation of the warm-Jupiter TOI-1130 system with CHEOPS and a photo-dynamical approach. A&A 689:A52
- Bozhilov V, Antonova D, Hobson MJ et al (2023) A 2:1 mean-motion resonance super-Jovian pair revealed by TESS, FEROS, and HARPS. ApJ 946(2):L36
- Bradbury J, Frostig R, Hawkins P et al (2018) JAX: composable transformations of Python+NumPy programs. http://github.com/jax-ml/jax
- Bryant EM, Bayliss D, Santerne A et al (2021) A transit timing variation observed for the longperiod extremely low-density exoplanet HIP 41378 f. MNRAS: Lett 504(1):L45–L50
- Canul EF, Velázquez H, Gómez Maqueo Chew Y (2021) Nauyaca: a new tool to determine planetary masses and orbital elements through transit timing analysis. AJ 162(6):262
- Carter JA, Agol E (2013) The quasiperiodic automated transit search algorithm. ApJ 765:132
- Carter JA, Winn JN (2009) Parameter estimation from time-series data with correlated errors: a wavelet-based method and its application to transit light curves. ApJ 704:51–67
- Carter JA, Yee JC, Eastman J, Gaudi BS, Winn JN (2008) Analytic approximations for transit light-curve observables, uncertainties, and covariances. ApJ 689:499–512
- Carter JA, Agol E, Chaplin WJ et al (2012) Kepler-36: a pair of planets with neighboring orbits and dissimilar densities. Science 337:556
- Chakraborty J, Kipping D (2022) Transit duration and timing variations from binary planets. MNRAS 519(2):2690–2700
- Chen C, Kong L, Li G, Tao M (2024) DeepTTV: deep learning prediction of hidden exoplanet from transit timing variations. arXiv e-prints arXiv:2409.04557

- Choksi N, Chiang E (2023) Exciting the transit timing variation phases of resonant sub-Neptunes. MNRAS 522(2):1914–1929
- Christiansen JL (2022) Five thousand exoplanets at the NASA exoplanet archive. Nat Astron 6(5):516–519
- Cloutier R, Greklek-McKeon M, Wurmser S et al (2023) Masses, revised radii, and a third planet candidate in the "inverted" planetary system around TOI-1266. MNRAS 527(3):5464–5483
- Cochran WD, Fabrycky DC, Torres G et al (2011) Kepler-18b, c, and d: a system of three planets confirmed by transit timing variations, light curve validation, warm-Spitzer photometry, and radial velocity measurements. ApJS 197:7
- Dai F, Masuda K, Beard C et al (2023) TOI-1136 is a young, coplanar, aligned planetary system in a pristine resonant chain. AJ 165(2):33
- Dai F, Goldberg M, Batygin K et al (2024) The prevalence of resonance among young, close-in planets. AJ 168(6):239
- Dawson RI, Johnson JA (2018) Origins of hot Jupiters. ARA&A 56:175–221
- Dawson RI, Johnson JA, Fabrycky DC et al (2014) Large eccentricity, low mutual inclination: the three-dimensional architecture of a hierarchical system of giant planets. ApJ 791:89
- Dawson RI, Huang CX, Lissauer JJ et al (2019) TOI-216b and TOI-216 c: two warm, large exoplanets in or slightly wide of the 2:1 orbital resonance. AJ 158(2):65
- Dawson RI, Huang CX, Brahm R et al (2021) Precise transit and radial-velocity characterization of a resonant pair: the warm Jupiter TOI-216c and eccentric warm Neptune TOI-216b. AJ 161(4):161
- Deck KM, Agol E (2015) Measurement of planet masses with transit timing variations due to synodic "chopping" effects. ApJ 802:116
- Deck KM, Agol E (2016) Transit timing variations for planets near eccentricity-type mean motion resonances. ApJ 821:96
- Deck KM, Holman MJ, Agol E et al (2012) Rapid dynamical chaos in an exoplanetary system. ApJ 755(1):L21
- Deck KM, Agol E, Holman MJ, Nesvorný D (2014) TTVFast: an efficient and accurate code for transit timing inversion problems. ApJ 787:132
- Delisle JB, Correia ACM, Leleu A, Robutel P (2017) Spin dynamics of close-in planets exhibiting large transit timing variations. A&A 605:A37
- Delrez L, Leleu A, Brandeker A et al (2023) Refining the properties of the TOI-178 system with CHEOPS and TESS. A&A 678:A200
- Dobbs-Dixon I, Agol E, Burrows A (2012) The impact of circumplantary jets on transit spectra and timing offsets for hot Jupiters. ApJ 751(2):87
- Dobrovolskis AR, Borucki WJ (1996a) Influence of Jovian extrasolar planets on transits of inner planets. In: AAS/division for planetary sciences meeting abstracts #28, vol 28. Bulletin of the American Astronomical Society, p 1112
- Dobrovolskis AR, Borucki WJ (1996b) Influence of Jovian extrasolar planets on transits of inner planets. In: Bulletin of the American Astronomical Society, BAAS, vol 28, p 1112
- Doyle LR, Carter JA, Fabrycky DC et al (2011) Kepler-16: a transiting circumbinary planet. Science 333:1602
- Duane S, Kennedy AD, Pendleton BJ, Roweth D (1987) Hybrid monte carlo. Phys Lett B 195(2):216–222
- Eastman J, Siverd R, Gaudi BS (2010) Achieving better than 1 minute accuracy in the heliocentric and barycentric Julian dates. PASP 122:935–946
- Eastman JD, Rodriguez JE, Agol E et al (2019) Exofastv2: a public, generalized, publication-quality exoplanet modeling code. https://doi.org/10.48550/ARXIV.1907.09480
- Eschen YNE, Bayliss D, Wilson TG et al (2024) Viewing the PLATO LOPS2 field through the lenses of TESS. MNRAS 535(2):1778–1795
- Fabrycky DC (2010) Non-Keplerian dynamics of exoplanets. In: Seager S (ed) Exoplanets. University of Arizona Press, Tucson, pp 217–238
- Fabrycky DC, Ford EB, Steffen JH et al (2012) Transit timing observations from Kepler. IV. Confirmation of four multiple-planet systems by simple physical models. ApJ 750:114

- Fermiano V, Saito RK, Ivanov VD et al (2024) The young exoplanetary system TOI-4562: confirming the presence of a third body in the system. A&A 690:L7
- Fletcher R (1987) Practical methods of optimization. Wiley, West Sussex
- Ford EB, Fabrycky DC, Steffen JH et al (2012a) Transit timing observations from Kepler. II. Confirmation of two multiplanet systems via a non-parametric correlation analysis. ApJ 750:113
- Ford EB, Ragozzine D, Rowe JF et al (2012b) Transit timing observations from Kepler. V. Transit timing variation candidates in the first sixteen months from polynomial models. ApJ 756:185
- Foreman-Mackey D, Agol E, Ambikasaran S, Angus R (2017) Fast and scalable gaussian process modeling with applications to astronomical time series. Astron J 154(6):220
- Foreman-Mackey D, Luger R, Agol E et al (2021) Exoplanet: gradient-based probabilistic inference for exoplanet data other astronomical time series. J Open Source Softw 6(62):3285
- Fortier A, Beck T, Benz W et al (2014) CHEOPS: a space telescope for ultra-high precision photometry of exoplanet transits. In: Space telescopes and instrumentation 2014: optical, infrared, and millimeter wave, Proceedings of SPIE, vol 9143, p 91432J
- Freudenthal J, von Essen C, Dreizler S et al (2018) Kepler Object of Interest Network: II. Photodynamical modelling of Kepler-9 over 8 years of transit observations. A&A 618:A41
- Freudenthal J, von Essen C, Ofir A et al (2019) Kepler object of interest network: III. Kepler-82f: a new non-transiting $21 \, M_{\oplus}$ planet from photodynamical modelling. A&A 628:A108
- Fukui A, Korth J, Livingston JH et al (2021) TOI-1749: an m dwarf with a trio of planets including a near-resonant pair. AJ 162(4):167
- Fulton BJ, Petigura EA (2018) The California-Kepler survey. VII. Precise planet radii leveraging Gaia DR2 reveal the stellar mass dependence of the planet radius gap. AJ 156(6):264
- Gao P, Zhang X (2020) Deflating super-puffs: impact of photochemical hazes on the observed mass-radius relationship of low-mass planets. ApJ 890(2):93
- García-Melendo E, López-Morales M (2011) Potential biases in the detection of planetary systems with large transit timing variations. MNRAS: Lett 417(1):L16–L20
- Gaudi BS, Seager S, Mennesson B et al (2020) The habitable exoplanet observatory (HabEx) mission concept study final report. arXiv e-prints arXiv:2001.06683
- Ge J, Zhang W, Zang W, Deng H et al (2022) ET white paper: to find the first Earth 2.0 arXiv:2206.06693
- Gibson NP, Aigrain S, Roberts S et al (2012) A Gaussian process framework for modelling instrumental systematics: application to transmission spectroscopy. MNRAS 419:2683–2694
- Gilbert EA, Barclay T, Schlieder JE et al (2020) The first habitable-zone Earth-sized planet from TESS. I. Validation of the TOI-700 system. AJ 160(3):116
- Gilbert EA, Vanderburg A, Rodriguez JE et al (2023) A second Earth-sized planet in the habitable zone of the M dwarf, TOI-700. ApJ 944(2):L35
- Gillon M, Jehin E, Lederer SM et al (2016) Temperate earth-sized planets transiting a nearby ultracool dwarf star. Nature 533(7602):221–224
- Gillon M, Triaud AHMJ, Demory BO et al (2017) Seven temperate terrestrial planets around the nearby ultracool dwarf star TRAPPIST-1. Nature 542(7642):456–460
- Ginzburg S, Schlichting HE, Sari R (2016) Super-Earth atmospheres: self-consistent gas accretion and retention. ApJ 825:29
- Goldberg M, Batygin K (2023) Dynamics and origins of the near-resonant Kepler planets. ApJ 948(1):12
- Gordon TA, Agol E, Foreman-Mackey D (2020) A fast, two-dimensional Gaussian process method based on Celerite: applications to transiting exoplanet discovery and characterization. AJ 160(5):240
- Greklek-McKeon M, Knutson HA, Vissapragada S et al (2023) Constraining the densities of the three Kepler-289 planets with transit timing variations. AJ 165(2):48
- Grimm SL, Demory BO, Gillon M et al (2018) The nature of the TRAPPIST-1 exoplanets. A&A 613:A68
- Hadden S (2019) First release of ttv2fast2furious. https://doi.org/10.5281/ZENODO.3356829

- Hadden S, Lithwick Y (2014) Densities and eccentricities of 139 Kepler planets from transit time variations. ApJ 787:80
- Hadden S, Lithwick Y (2016) Numerical and analytical modeling of transit timing variations. ApJ 828:44
- Hadden S, Lithwick Y (2017) Kepler planet masses and eccentricities from TTV analysis. AJ 154(1):5
- Hadden S, Tamayo D (2022) celmech: a python package for celestial mechanics. AJ 164(5):179
- Hadden S, Barclay T, Payne MJ, Holman MJ (2019) Prospects for TTV detection and dynamical constraints with TESS. AJ 158(4):146
- Hamann A, Montet BT, Fabrycky DC, Agol E, Kruse E (2019) K2-146: discovery of planet c, precise masses from transit timing, and observed precession. AJ 158(3):133
- Hattori S, Garcia L, Murray C et al (2024) exoplanet-dev/jaxoplanet: astronomical time series analysis with JAX. https://doi.org/10.5281/ZENODO.10736936
- Hébrard G, Díaz RF, Correia ACM et al (2020) Discovery and characterization of the exoplanets WASP-148b and c: a transiting system with two interacting giant planets. A&A 640:A32
- Heitzmann A, Zhou G, Quinn SN et al (2023) TOI-4562b: a highly eccentric temperate jupiter analog orbiting a young field star. AJ 165(3):121
- Heyl JS, Gladman BJ (2007) Using long-term transit timing to detect terrestrial planets. MNRAS 377:1511–1519
- Hobson MJ, Trifonov T, Henning T et al (2023) TOI-199 b: a well-characterized 100-day transiting warm giant planet with TTVs seen from Antarctica. AJ 166(5):201
- Hoffman MD, Gelman A et al (2014) The No-U-Turn sampler: adaptively setting path lengths in Hamiltonian Monte Carlo. J Mach Learn Res 15(1):1593–1623
- Holczer T, Mazeh T, Nachmani G et al (2016) Transit timing observations from Kepler. IX. Catalog of the full long-cadence data set. ApJS 225:9
- Holman MJ, Murray NW (2005) The use of transit timing to detect terrestrial-mass extrasolar planets. Science 307:1288–1291
- Holman MJ, Fabrycky DC, Ragozzine D et al (2010) Kepler-9: a system of multiple planets transiting a sun-like star, confirmed by timing variations. Science 330:51
- Howard WS, Kowalski AF, Flagg L et al (2023) Characterizing the near-infrared spectra of flares from TRAPPIST-1 during JWST transit spectroscopy observations. ApJ 959(1):64
- Huang CX, Quinn SN, Vanderburg A et al (2020) TESS spots a hot Jupiter with an inner transiting Neptune. ApJ 892(1):L7
- Ikhsan MI, Arifyanto MI, Hidayat T (2024) Machine learning implementation on TTV analysis using TTVFast. J Phys Conf Ser 2734(1):012010
- Ioannidis P, Huber KF, Schmitt JHMM (2016) How do starspots influence the transit timing variations of exoplanets? Simulations of individual and consecutive transits. A&A 585:A72
- Ivshina ES, Winn JN (2022) TESS transit timing of hundreds of hot Jupiters. ApJS 259(2):62
- Jackson JM, Dawson RI, Zalesky J (2019) The origin of Kepler-419b: a path to tidal migration via four-body secular interactions. AJ 157(4):166
- Johansen A, Davies MB, Church RP, Holmelin V (2012) Can planetary instability explain the Kepler dichotomy? ApJ 758(1):39
- Jones SE, Stefánsson G, Masuda K et al (2024) TOI-2015 b: a warm Neptune with transit timing variations orbiting an active mid-type M dwarf. Astron J 168(2):93
- Jontof-Hutter D (2019) The compositional diversity of low-mass exoplanets. Annu Rev Earth Planet Sci 47(1):141–171
- Jontof-Hutter D, Ford EB, Rowe JF et al (2016) Secure mass measurements from transit timing: 10 Kepler exoplanets between 3 and 8 M_{\oplus} with diverse densities and incident fluxes. ApJ 820:39
- Jontof-Hutter D, Wolfgang A, Ford EB et al (2021) Following up the Kepler field: masses of targets for transit timing and atmospheric characterization. AJ 161(5):246
- Jontof-Hutter D, Dalba PA, Livingston JH (2022) TESS observations of Kepler systems with transit timing variations. AJ 164(2):42
- Judkovsky Y, Ofir A, Aharonson O (2020) Light-curve evolution due to secular dynamics and the vanishing transits of KOI 120.01. AJ 160(4):195

- Judkovsky Y, Ofir A, Aharonson O (2022a) An accurate 3D analytic model for exoplanetary photometry, radial velocity, and astrometry. AJ 163(2):90
- Judkovsky Y, Ofir A, Aharonson O (2022b) Physical properties and impact parameter variations of Kepler planets from analytic light-curve modeling. AJ 163(2):91
- Judkovsky Y, Ofir A, Aharonson O (2023) The advantages of global photometric models in fitting transit variations. AJ 166(6):256
- Judkovsky Y, Ofir A, Aharonson O (2024) Kepler multitransiting system physical properties and impact parameter variations. AJ 167(3):103
- Kaye L, Vissapragada S, Günther MN et al (2021) Transit timings variations in the three-planet system: TOI-270. MNRAS 510(4):5464–5485
- Kipping D (2020) The exomoon corridor: half of all exomoons exhibit TTV frequencies within a narrow window due to aliasing. MNRAS 500(2):1851–1857
- Kipping D, Teachey A (2020) Impossible moons—transit timing effects that cannot be due to exomoon. Serbian Astron J (201):25–37
- Kipping D, Yahalomi DA (2022) A search for transit timing variations within the exomoon corridor using Kepler data. MNRAS 518(3):3482–3493
- Kipping D, Nesvorný D, Hartman J et al (2019) A resonant pair of warm giant planets revealed by TESS. MNRAS 486(4):4980–4986
- Kipping DM (2014) Characterizing distant worlds with asterodensity profiling. MNRAS 440:2164–2184
- Korth J, Gandolfi D, Šubjak J et al (2023) TOI-1130: a photodynamical analysis of a hot Jupiter in resonance with an inner low-mass planet. A&A 675:A115
- Korth J, Chaturvedi P, Parviainen H et al (2024) TOI-1408: discovery and photodynamical modeling of a small inner companion to a hot Jupiter revealed by TTVs. ApJL 971(2):L28
- Kostov VB, McCullough PR, Hinse TC et al (2013) A gas giant circumbinary planet transiting the F star primary of the eclipsing binary star KIC 4862625 and the independent discovery and characterization of the two transiting planets in the Kepler-47 system. ApJ 770:52
- Kostov VB, McCullough PR, Carter JA et al (2014) Kepler-413b: a slightly misaligned, Neptunesize transiting circumbinary planet. ApJ 784:14
- Kovács G, Zucker S, Mazeh T (2002) A box-fitting algorithm in the search for periodic transits. A&A 391(1):369–377
- Lacedelli G, Malavolta L, Borsato L et al (2020) An unusually low density ultra-short period super-Earth and three mini-Neptunes around the old star TOI-561. MNRAS 501(3):4148–4166
- Lammers C, Winn JN (2024) The six-planet resonant chain of HD 110067. ApJ 968(1):L12
- Langford Z, Agol E (2024) A differentiable N-body code for transit timing and dynamical modelling—II. Photodynamics. arXiv preprint arXiv:2410.03874
- Laughlin G, Chambers JE (2001) Short-term dynamical interactions among extrasolar planets. ApJ 551:L109–L113
- Le Verrier UJ (1877) Tables du mouvement de Neptune fondees sur la comparaison de la theorie avec les observations. Annales de l'Observatoire de Paris 14:1
- Lee EJ, Chiang E (2016) Breeding super-Earths and birthing super-puffs in transitional disks. ApJ 817:90
- Leleu A, Alibert Y, Hara NC et al (2021) Six transiting planets and a chain of Laplace resonances in TOI-178. A&A 649:A26
- Leleu A, Delisle JB, Mardling R et al (2022) Alleviating the transit timing variation bias in transit surveys: II. RIVERS: twin resonant Earth-sized planets around Kepler-1972 recovered from a Kepler false positive. A&A 661:A141
- Leleu A, Delisle JB, Udry S et al (2023) Removing biases on the density of sub-Neptunes characterised via transit timing variations: update on the mass-radius relationship of 34 Kepler planets. A&A 669:A117
- Leleu A, Delisle JB, Burn R et al (2024a) Resonant sub-Neptunes are puffier. A&A 687:L1
- Leleu A, Delisle JB, Delrez L et al (2024b) Photo-dynamical characterisation of the TOI-178 resonant chain: exploring the robustness of transit-timing variations and radial velocity mass characterisations. A&A 688:A211

- Li R, Chiang E, Choksi N, Dai F (2024) The resonant remains of broken chains from major and minor mergers. https://doi.org/10.48550/ARXIV.2408.10206
- Liang Y, Robnik J, Seljak U (2021) Kepler-90: giant transit-timing variations reveal a super-puff. AJ 161(4):202
- Libby-Roberts JE, Berta-Thompson ZK, Désert JM et al (2020) The featureless transmission spectra of two super-puff planets. AJ 159(2):57
- Lindor B, Agol E (2024) Modeling the solar system as an observed multi-transit system I: characterization limits from analytic timing variations. https://doi.org/10.48550/ARXIV.2407. 13154
- Linial I, Gilbaum S, Sari R (2018) Modal decomposition of TTV: inferring planet masses and eccentricities. ApJ 860(1):16
- Lissauer JJ, Fabrycky DC, Ford EB et al (2011) A closely packed system of low-mass, low-density planets transiting Kepler-11. Nature 470:53–58
- Lissauer JJ, Rowe JF, Jontof-Hutter D et al (2024) Updated catalog of Kepler planet candidates: focus on accuracy and orbital periods. Planet Sci J 5(6):152
- Lithwick Y, Xie J, Wu Y (2012) Extracting planet mass and eccentricity from TTV data. ApJ 761:122
- Luger R, Sestovic M, Kruse E et al (2017) A seven-planet resonant chain in TRAPPIST-1. Nat Astron 1(6):0129
- Luque R, Osborn HP, Leleu A et al (2023) A resonant sextuplet of sub-Neptunes transiting the bright star HD 110067. Nature 623(7989):932–937
- MacDonald MG, Shakespeare CJ, Ragozzine D (2021) A five-planet resonant chain: reevaluation of the Kepler-80 system. AJ 162(3):114
- MacDonald MG, Feil L, Quinn T, Rice D (2022) Confirming the 3:2 resonance chain of K2-138. AJ 163(4):162
- MacDonald MG, Polania Vivas MS, D'Angiolillo S, Fernandez AN, Quinn T (2023) exoMMR: a new python package to confirm and characterize mean motion resonances. AJ 166(3):94
- Malavolta L, Borsato L, Granata V et al (2017) The Kepler-19 system: a thick-envelope super-Earth with two Neptune-mass companions characterized using radial velocities and transit timing variations. AJ 153(5):224
- Martin DV (2017) Circumbinary planets—II. When transits come and go. MNRAS 465:3235–3253 Martin DV, Fabrycky DC, Montet BT (2019) Transits of inclined exomoons—hide and seek and an application to Kepler-1625. ApJL 875(2):L25
- Martioli E, Hébrard G, Correia ACM, Laskar J, Lecavelier des Etangs A (2021) New constraints on the planetary system around the young active star AU Mic: two transiting warm Neptunes near mean-motion resonance. A&A 649:A177
- Masuda K (2014) Very low density planets around Kepler-51 revealed with transit timing variations and an anomaly similar to a planet-planet eclipse event. ApJ 783:53
- Masuda K, Tamayo D (2020) Revisiting the architecture of the KOI-89 system. AJ 160(5):224
- Masuda K, Hirano T, Taruya A, Nagasawa M, Suto Y (2013) Characterization of the KOI-94 system with transit timing variation analysis: implication for the planet-planet eclipse. ApJ 778(2):185
- Masuda K, Libby-Roberts JE, Livingston JH et al (2024) A fourth planet in the Kepler-51 system revealed by transit timing variations. AJ 168(6):294
- Mayer P (1971) Eclipsing variable IU Aurigae. Bull Astron Inst Czechoslov 22:168
- Mazeh T, Nachmani G, Holczer T et al (2013) Transit timing observations from Kepler. VIII. Catalog of transit timing measurements of the first twelve quarters. ApJS 208:16
- McKee BJ, Montet BT (2023) Transit depth variations reveal TOI-216 b to be a super-puff. AJ 165(6):236
- McKee BJ, Montet BT, Yee SW et al (2025) A planet candidate orbiting near the hot jupiter TOI-2818 b inferred through transit timing. ApJ 981(2):106
- Meschiari S, Laughlin GP (2010) Systemic: a testbed for characterizing the detection of extrasolar planets. II. Numerical approaches to the transit timing inverse problem. ApJ 718:543–550
- Millholland S (2019) Tidally induced radius inflation of sub-Neptunes. ApJ 886(1):72

- Millholland S, Wang S, Laughlin G (2016) On the detection of non-transiting hot Jupiters in multiple-planet systems. ApJ 823(1):L7
- Millholland SC, He MY, Ford EB et al (2021) Evidence for a nondichotomous solution to the Kepler dichotomy: mutual inclinations of Kepler planetary systems from transit duration variations. AJ 162(4):166
- Mills SM, Fabrycky DC (2017) Kepler-108: a mutually inclined giant planet system. AJ 153(1):45 Mills SM, Mazeh T (2017) The planetary mass-radius relation and its dependence on orbital period as measured by transit timing variations and radial velocities. ApJ 839:L8
- Mills SM, Fabrycky DC, Migaszewski C et al (2016) A resonant chain of four transiting, sub-Neptune planets. Nature 533:509–512
- Miralda-Escudé J (2002) Orbital perturbations of transiting planets: a possible method to measure stellar quadrupoles and to detect Earth-mass planets. ApJ 564:1019–1023
- Montet BT, Yee JC, Penny MT (2017) Measuring the galactic distribution of transiting planets with WFIRST. PASP 129(4):044401
- NASA Exoplanet Science Institute (2020) Planetary systems table. https://doi.org/10.26133/ NEA12
- Nascimbeni V, Borsato L, Leonardi P et al (2024) The K2-24 planetary system revisited by CHEOPS. A&A 690:A349
- Nesvorný D, Chrenko O, Flock M (2022) TOI-216: resonant constraints on planet migration. ApJ 925(1):38
- Nesvorný D (2009) Transit timing variations for eccentric and inclined exoplanets. ApJ 701:1116–1122
- Nesvorný D, Beaugé C (2010) Fast inversion method for determination of planetary parameters from transit timing variations. ApJ 709:L44–L48
- Nesvorný D, Morbidelli A (2008) Mass and orbit determination from transit timing variations of exoplanets. ApJ 688:636-646
- Nesvorný D, Vokrouhlický D (2014) The effect of conjunctions on the transit timing variations of exoplanets. ApJ 790:58
- Nesvorný D, Vokrouhlický D (2016) Dynamics and transit variations of resonant exoplanets. ApJ 823:72
- Nesvorný D, Kipping DM, Buchhave LA et al (2012) The detection and characterization of a nontransiting planet by transit timing variations. Science 336:1133
- Nesvorný D, Kipping D, Terrell D et al (2013) KOI-142, the king of transit variations, is a pair of planets near the 2:1 resonance. ApJ 777:3
- Nicholson BA, Aigrain S, Eisner NL et al (2024) HD152843 b & c: the masses and orbital periods of a sub-Neptune and a superpuff Neptune. MNRAS 532(4):4632–4644
- Ofir A, Xie JW, Jiang CF, Sari R, Aharonson O (2018) A spectral approach to transit timing variations. ApJS 234(1):9
- Ofir A, Yoffe G, Aharonson O (2025) Planetary mass determinations from a simplified photodynamical model—application to the complete Kepler dataset. AJ 169:90
- Orosz JA, Welsh WF, Haghighipour N et al (2019) Discovery of a third transiting planet in the Kepler-47 circumbinary system. AJ 157(5):174
- Osborn HP, Bonfanti A, Gandolfi D et al (2022) Uncovering the true periods of the young sub-Neptunes orbiting TOI-2076. A&A 664:A156
- Oshagh M, Santos NC, Boisse I et al (2013) Effect of stellar spots on high-precision transit lightcurve. A&A 556:A19
- Otegi JF, Bouchy F, Helled R (2020) Revisited mass-radius relations for exoplanets below 120 $M_{\oplus}.$ A&A 634:A43
- Pál A, Kocsis B (2008) Periastron precession measurements in transiting extrasolar planetary systems at the level of general relativity. MNRAS 389:191–198
- Pepe F, Cristiani S, Rebolo R et al (2021) ESPRESSO at VLT: on-sky performance and first results. A&A 645:A96
- Peterson MS, Benneke B, Collins K et al (2023) A temperate earth-sized planet with tidal heating transiting an M6 star. Nature 617(7962):701–705

- Petit AC, Petigura EA, Davies MB, Johansen A (2020) Resonance in the K2-19 system is at odds with its high reported eccentricities. MNRAS 496(3):3101–3111
- Plavchan P, Barclay T, Gagné J et al (2020) A planet within the debris disk around the pre-main-sequence star au microscopii. Nature 582(7813):497–500
- Pozuelos FJ, Timmermans M, Rackham BV et al (2023) A super-Earth and a mini-Neptune near the 2:1 MMR straddling the radius valley around the nearby mid-M dwarf TOI-2096. A&A 672:A70
- Price EM, Rogers LA (2014) Transit light curves with finite integration time: fisher information analysis. ApJ 794:92
- Quinn SN, Becker JC, Rodriguez JE et al (2019) Near-resonance in a system of sub-Neptunes from TESS. AJ 158(5):177
- Quirrenbach A, Amado PJ, Caballero JA et al (2014) CARMENES instrument overview. In: Ramsay SK, McLean IS, Takami H (eds) Ground-based and airborne instrumentation for astronomy V. SPIE
- Ragozzine D, Wolf AS (2009) Probing the interiors of very hot Jupiters using transit light curves. ApJ 698:1778–1794
- Rauer H, Catala C, Aerts C et al (2014) The PLATO 2.0 mission. Exp Astron 38:249-330
- Rein H, Liu SF (2012) REBOUND: an open-source multi-purpose N-body code for collisional dynamics. A&A 537:A128
- Rein H, Tamayo D (2016) Second-order variational equations forn-body simulations. MNRAS 459(3):2275–2285
- Rice M, Wang XY, Wang S et al (2023) Evidence for low-level dynamical excitation in nearresonant exoplanet systems. AJ 166(6):266
- Ricker GR, Winn JN, Vanderspek R et al (2014) Transiting exoplanet survey satellite (TESS). In: Space telescopes and instrumentation 2014: optical, infrared, and millimeter wave. Proceedings of SPIE, vol 9143, p 914320
- Ricker GR, Winn JN, Vanderspek R et al (2015) Transiting exoplanet survey satellite (TESS). J Astron Telescopes Instrum Syst 1(1):014003
- Rowe JF, Coughlin JL, Antoci V et al (2015) Planetary candidates observed by Kepler. V. planet sample from Q1–Q12 (36 months). ApJS 217(1):16
- Rustamkulov Z, Sing DK, Mukherjee S et al (2023) Early Release Science of the exoplanet WASP-39b with JWST NIRSpec PRISM. Nature 614(7949):659–663
- Saad-Olivera X, Nesvorný D, Kipping DM, Roig F (2017) Masses of Kepler-46b, c from transit timing variations. AJ 153(4):198
- Saad-Olivera X, Costa de Souza A, Roig F, Nesvorný D (2018) Masses of the Kepler-419 planets from transit timing variations analysis. MNRAS 482(4):4965–4971
- Schmitt JR, Agol E, Deck KM et al (2014) Planet hunters. VII. Discovery of a new low-mass, low-density planet (PH3 C) orbiting Kepler-289 with mass measurements of two additional planets (PH3 B and D). ApJ 795:167
- Schneider J (2003) Multi-planet system detection by transits. In: Combes F, Barret D, Contini T, Pagani L (eds) SF2A-2003: Semaine de l'Astrophysique Francaise, p 149
- Schneider J (2004) Multi-planet system detection with Eddington. In: Favata F, Aigrain S, Wilson A (eds) Stellar structure and habitable planet finding. ESA special publication, vol 538, pp 407–410
- Seager S, Mallén-Ornelas G (2003) A unique solution of planet and star parameters from an extrasolar planet transit light curve. ApJ 585:1038–1055
- Shahaf S, Mazeh T, Zucker S, Fabrycky D (2021) Systematic search for long-term transit duration changes in Kepler transiting planets. MNRAS 505(1):1293–1310
- Siegel JC, Rogers LA (2022) Mass upper bounds for over 50 Kepler planets using low-S/N transit timing variations. AJ 164(4):139
- Steffen J (2006) Detecting new planets in transiting systems. PhD thesis, University of Washington Steffen JH (2016) Sensitivity bias in the mass-radius distribution from transit timing variations and radial velocity measurements. Mon Not R Astron Soc 457(4):4384–4392
- Steffen JH, Agol E (2005) An analysis of the transit times of TrES-1b. MNRAS 364:L96-L100

- Steffen JH, Fabrycky DC, Ford EB et al (2012a) Transit timing observations from Kepler—III. Confirmation of four multiple planet systems by a Fourier-domain study of anticorrelated transit timing variations. MNRAS 421:2342–2354
- Steffen JH, Ragozzine D, Fabrycky DC et al (2012b) Kepler constraints on planets near hot Jupiters. Proc Natl Acad Sci 109(21):7982–7987
- Sterken C (2005) The O-C diagram: basic procedures. In: Sterken C (ed) The light-time effect in astrophysics: causes and cures of the O-C diagram. Astronomical society of the pacific conference series, vol 335, p 3
- Sun L, Ioannidis P, Gu S et al (2019) Kepler-411: a four-planet system with an active host star. A&A 624:A15
- Sun L, Ioannidis P, Gu S et al (2022) A highly mutually inclined compact warm-Jupiter system KOI-984? MNRAS 512(3):4604–4617
- Szabó GM, Gandolfi D, Brandeker A et al (2021) The changing face of AU MIC b: stellar spots, spin-orbit commensurability, and transit timing variations as seen by CHEOPS and TESS. A&A 654:A159
- Szabó GM, Garai Z, Brandeker A et al (2022) Transit timing variations of AU Microscopii b and c. A&A 659:L7
- Szabó GM, Pál A, Derekas A et al (2012) Spin-orbit resonance, transit duration variation and possible secular perturbations in KOI-13. MNRAS: Lett 421(1):L122–L126
- Tamayo D, Gilbertson C, Foreman-Mackey D (2020) Stability constrained characterization of multiplanet systems. MNRAS 501(4):4798–4811
- Teachey A, Kipping DM (2018) Evidence for a large exomoon orbiting Kepler-1625b. Sci Adv 4(10):eaav1784
- Teyssandier J, Libert AS (2020) Transit timing variation signature of planet migration: the case of K2-24. A&A 643:A11
- Thompson SE, Coughlin JL, Hoffman K et al (2018) Planetary candidates observed by Kepler. VIII. A fully automated catalog with measured completeness and reliability based on data release 25. ApJS 235(2):38
- Tinetti G, Drossart P, Eccleston P et al (2016) The science of ARIEL (Atmospheric Remote-sensing Infrared Exoplanet Large-survey). In: MacEwen HA, Fazio GG, Lystrup M et al (eds) Space telescopes and instrumentation 2016: optical, infrared, and millimeter wave. SPIE, vol 9904, p 99041X
- Tinetti G, Drossart P, Eccleston P et al (2018) A chemical survey of exoplanets with ARIEL. Exp Astron 46(1):135–209
- Trifonov T, Brahm R, Espinoza N et al (2021) A pair of warm giant planets near the 2:1 mean motion resonance around the k-dwarf star TOI-2202. AJ 162(6):283
- Trifonov T, Brahm R, Jordán A et al (2023) TOI-2525 b and c: a pair of massive warm giant planets with strong transit timing variations revealed by TESS. AJ 165(4):179
- Turtelboom EV, Weiss LM, Dressing CD et al (2022) The TESS-Keck survey. XI. Mass measurements for four transiting sub-Neptunes orbiting K dwarf TOI–1246. AJ 163(6):293
- Ulrich RK (1986) Determination of stellar ages from asteroseismology. ApJ 306:L37–L40
- Van Eylen V, Albrecht S (2015) Eccentricity from transit photometry: small planets in Kepler multi-planet systems have low eccentricities. ApJ 808(2):126
- van Eylen V, Albrecht S, Huang X et al (2019) The orbital eccentricity of small planet systems. AJ 157(2):61
- Vissapragada S, Jontof-Hutter D, Shporer A et al (2020) Diffuser-assisted infrared transit photometry for four dynamically interacting Kepler systems. AJ 159(3):108
- Vivien HG, Hoyer S, Deleuil M et al (2024) New ephemerides and detection of transit-timing variations in the K2-138 system using high-precision CHEOPS photometry. A&A 688:A192
- Vítková M, Brahm R, Trifonov T et al (2025) TOI-4504: exceptionally large transit timing variations induced by two resonant warm gas giants in a three planet system. ApJL 978(2):L22
- von Essen C, Ofir A, Dreizler S et al (2018) Kepler object of interest network: I. First results combining ground- and space-based observations of Kepler systems with transit timing variations. A&A 615:A79

- Wang G, Espinoza N (2023) A blind search for transit depth variability with TESS. AJ 167(1):1
- Wang L, Dai F (2019) Dusty outflows in planetary atmospheres: understanding "super-puffs" and transmission spectra of sub-Neptunes. ApJ 873(1):L1
- Weiss LM, Marcy GW, Rowe JF et al (2013) The mass of KOI-94d and a relation for planet radius, mass, and incident flux. ApJ 768(1):14
- Weiss LM, Fabrycky DC, Agol E et al (2020) The discovery of the long-period, eccentric planet Kepler-88 d and system characterization with radial velocities and photodynamical analysis. AJ 159(5):242
- Weiss LM, Dai F, Huber D et al (2021) The TESS-Keck Survey. II. An ultra-short-period rocky planet and its siblings transiting the galactic thick-disk star TOI-561. AJ 161(2):56
- Welsh WF, Orosz JA, Carter JA et al (2012) Transiting circumbinary planets Kepler-34 b and Kepler-35 b. Nature 481:475–479
- Wilson C (1985) The great inequality of Jupiter and Saturn: from Kepler to Laplace. Arch Hist Exact Sci 33:15–290
- Winn JN (2010) Transits and occultations. https://doi.org/10.48550/ARXIV.1001.2010
- Wittrock JM, Dreizler S, Reefe MA et al (2022) Transit timing variations for AU microscopii b and c. AJ 164(1):27
- Wittrock JM, Plavchan PP, Cale BL et al (2023) Validating AU microscopii d with transit timing variations. AJ 166(6):232
- Wolfgang A, Laughlin G (2012) The effect of population-wide mass-to-radius relationships on the interpretation of Kepler and HARPS super-earth occurrence rates. ApJ 750(2):148
- Wolszczan A (1994) Confirmation of Earth-Mass planets orbiting the millisecond pulsar PSR B1257+12. Science 264:538-542
- Wu DH, Rice M, Wang S (2023) Evidence for hidden nearby companions to hot Jupiters. AJ 165(4):171
- Wu Y, Malhotra R, Lithwick Y (2024) Repelling planet pairs by ping-pong scattering. ApJ 971(1):5
 Xie JW (2013) Transit timing variation of near-resonance planetary pairs: confirmation of 12 multiple-planet systems. ApJS 208:22
- Xie JW (2014) Transit timing variation of near-resonance planetary pairs. II. Confirmation of 30 planets in 15 multiple-planet systems. ApJS 210:25
- Yahalomi DA, Kipping D, Nesvorný D et al (2023) Not-so-fast Kepler-1513: a perturbing planetary interloper in the exomoon corridor. MNRAS 527(1):620–639
- Yahalomi DA, Kipping D, Agol E, Nesvorny D (2024) The exoplanet edge: planets don't induce observable TTVs faster than half their orbital period. https://doi.org/10.48550/ARXIV.2411. 09752
- Yee SW, Tamayo D, Hadden S, Winn JN (2021) How close are compact multiplanet systems to the stability limit? AJ 162(2):55
- Yoffe G, Ofir A, Aharonson O (2021) A simplified photodynamical model for planetary mass determination in low-eccentricity multitransiting systems. ApJ 908(1):114
- Zeng L, Jacobsen SB, Sasselov DD et al (2019) Growth model interpretation of planet size distribution. Proc Natl Acad Sci 116(20):9723–9728
- Zhang Z, Wang W, Ma X et al (2024) Constraining the presence of companion planets in hot Jupiter planetary systems using transit-timing variation observations from TESS. ApJS 275(2):32
- Zhu W (2020) On the patterns observed in Kepler multi-planet systems. AJ 159(5):188
- Zhu W, Petrovich C, Wu Y, Dong S, Xie J (2018) About 30% of sun-like stars have Kepler-like planetary systems: a study of their intrinsic architecture. ApJ 860(2):101
- Zingales T, Malavolta L, Borsato L et al (2025) A joint effort to discover and characterize two resonant mini Neptunes around TOI-1803 with TESS, HARPS-N and CHEOPS. A&A 695:A273